Approved for public release; distribution is unlimited.

Intraseasonal Relationships Between Tropical Heating and Extratropical Jets

by

Michael T. Neith
Lieutenant, United States Navy
B.S., Allentown College of
St. Francis de Sales, 1986

Submitted in partial fulfillment
of the requirements for the degree of

MASTER OF SCIENCE IN METEOROLOGY AND
PHYSICAL OCEANOGRAPHY

from the

NAVAL POSTGRADUATE SCHOOL
DECEMBER 1992

UNCLASSIFIED

SECURITY CLASSIFICATION OF THIS PAGE

REPORT DOCUMENTATION PAGE

1a. REPORT SECURITY CLASSIFICATION UNCLASSIFIED	1b. RESTRICTIVE MARKINGS
2a. SECURITY CLASSIFICATION AUTHORITY	3. DISTRIBUTION/AVAILABILITY OF REPORT Approved for public release; distribution is unlimited.
2b. DECLASSIFICATION/DOWNGRADING SCHEDULE	
4. PERFORMING ORGANIZATION REPORT NUMBER(S)	5. MONITORING ORGANIZATION REPORT NUMBER(S)
6a. NAME OF PERFORMING ORGANIZATION Naval Postgraduate School 6b. OFFICE SYMBOL (*If applicable*) 55	7a. NAME OF MONITORING ORGANIZATION Naval Postgraduate School
6c. ADDRESS (*City, State, and ZIP Code*) Monterey, CA 93943-5000	7b. ADDRESS (*City, State, and ZIP Code*) Monterey, CA 93943-5000
8a. NAME OF FUNDING/SPONSORING ORGANIZATION 8b. OFFICE SYMBOL (*If applicable*)	9. PROCUREMENT INSTRUMENT IDENTIFICATION NUMBER
8c. ADDRESS (*City, State, and ZIP Code*)	10. SOURCE OF FUNDING NUMBERS Program Element No / Project No. / Task No / Work Unit Accession Number

11. TITLE (*Include Security Classification*)
INTRASEASONAL RELATIONSHIPS BETWEEN TROPICAL HEATING AND EXTRATROPICAL JETS

12. PERSONAL AUTHOR(S) Michael T. Neith

13a. TYPE OF REPORT	13b. TIME COVERED	14. DATE OF REPORT (*year, month, day*)	15. PAGE COUNT
Master's Thesis	From To	1992, December, 14	109

16. SUPPLEMENTARY NOTATION
The views expressed in this thesis are those of the author and do not reflect the official policy or position of the Department of Defense or the U.S. Government.

17. COSATI CODES			18. SUBJECT TERMS (*continue on reverse if necessary and identify by block number*)
FIELD	GROUP	SUBGROUP	Teleconnections; Intraseasonal Oscillations; Tropical Heating; Extratropical Jets.

19. ABSTRACT (*continue on reverse if necessary and identify by block number*)

Intraseasonal variations of the northern midlatitude circulation and their relationships with the global tropical heating field are investigated using climate model fields. The greatest intraseasonal variance in the midlatitude flow is found in the vicinity of the time mean jets, and in the areas immediately downstream of these jet exits. The model kinetic energy field associated with these jets shows a clear 30-60 day variation and eastward propagation within and between the different jet regions. This intraseasonal behavoir is found to be well correlated with heating anomalies in specific parts of the global tropics.

For each of these jet regions, we use a simple composite analysis to identify the global heating patterns associated with periods of strong and weak flow. For the North Pacific jet, strong flow occurs during and after periods of positive heating anomalies in the tropical western and central Pacific, and negative heating anomalies in the Indian Ocean. Conversely, The North Pacific flow is weak when these heating anomalies are reversed. The North Atlantic jet shows comparable relationships, with positive heating anomalies in the tropical western and eastern Pacific, and negative heating anomalies in the tropical Indian and Atlantic Oceans, before and during periods of strong flow.

These intraseasonal teleconnections between individual jets and the global tropical heating field are especially clear for the North Pacific and North Atlantic jets. In addition to relatively direct forcing from nearby tropical heat sources, the jets may be influenced by relatively remote tropical heat sources, whose signals propagate through upstream jets. These intraseasonal teleconnections between the global tropical heating field and the North Pacific and North Atlantic jets may have important implications for extended range forecasting for North America and Europe.

20. DISTRIBUTION/AVAILABILITY OF ABSTRACT	21. ABSTRACT SECURITY CLASSIFICATION
☒ UNCLASSIFIED/UNLIMITED ☐ SAME AS REPORT ☐ DTIC USERS	UNCLASSIFIED
22a. NAME OF RESPONSIBLE INDIVIDUAL James Thomas Murphree	22b. TELEPHONE (*Include Area code*) (408) 646-2723 — 22c. OFFICE SYMBOL MR/Me

DD FORM 1473, 84 MAR — 83 APR edition may be used until exhausted / All other editions are obsolete — SECURITY CLASSIFICATION OF THIS PAGE: UNCLASSIFIED

ABSTRACT

Intraseasonal variations of the northern midlatitude circulation and their relationships with the global tropical heating field are investigated using climate model fields. The greatest intraseasonal variance in the midlatitude flow is found in the vicinity of the time mean jets, and in the areas immediately downstream of these jet exits. The model kinetic energy field associated with these jets shows a clear 30-60 day variation and eastward propagation within and between the different jet regions. This intraseasonal behavior is found to be well correlated with heating anomalies in specific parts of the global tropics.

For each of the jet regions, we use a simple composite analysis to identify the global heating patterns associated with periods of strong and weak flow. For the North Pacific jet, strong flow occurs during and after periods of positive heating anomalies in the tropical western and central Pacific, and negative heating anomalies in the Indian Ocean. Conversely, the North Pacific flow is weak when these heating anomalies are reversed. The North Atlantic jet shows comparable relationships, with positive heating anomalies in the tropical western and eastern Pacific, and negative heating anomalies in the tropical Indian and Atlantic Oceans, before and during periods of strong flow.

These intraseasonal teleconnections between individual jets and the global tropical heating field are especially clear for the North Pacific and North Atlantic jets. In addition to relatively direct forcing from nearby tropical heat sources, the jets may be influenced by relatively remote tropical heat sources, whose signals propagate through upstream jets. These intraseasonal teleconnections between the global tropical heating field and the North Pacific and North Atlantic jets may have important implications for extended range forecasting in North America and Europe.

LIST OF SYMBOLS AND ACRONYMS

AF - Africa

AT - Atlantic Ocean

C - positive POLR (cooling) anomalies

CHT - cumulus heating

CP - central Pacific Ocean

DERF - dynamical extended range forecasting

EA - East Asia

ECMWF - European Center for Medium Range Forecasts

EP - eastern Pacific Ocean

EU - Eurasia

FFT - Fast Fourier Transform

FNOC - Fleet Numerical Oceanography Center

GCM - general circulation model

GMT - Greenwich Mean Time

H - negative POLR (heating) anomalies

IO - Indian Ocean

ITCZ - Inter-Tropical Convergence Zone

KE - kinetic energy

m - meter

mb - millibar

MJO - Madden-Julian Oscillation

NA - North America

NAT - North Atlantic Ocean

NOGAPS - Navy Operational Global Atmospheric Prediction System

NP - North Pacific Ocean

OLR - outgoing longwave radiation

PKE - processed kinetic energy

POLR - processed outgoing longwave radiation

s - second

SACZ - South Atlantic Convergence Zone

SPCZ - South Pacific Convergence Zone

T - transition between tropical heating and cooling

T49 - triangular 49 truncation

U200 - 200mb zonal wind

U250 - 250mb zonal wind

V200 - 200mb meridional wind

VHT - vertically-integrated heating

W - Watts

WESTPAC - western Pacific Ocean (5°N - 25°N)

WP - western Pacific Ocean (30°S - 30°N)

χ - velocity potential

Ψ - streamfunction

ACKNOWLEDGMENTS

I am grateful to Prof. J. T. Murphree for his valuable advice and generous assistance in completing this study. Discussions with Prof. P. Harr were very helpful in clarifying some of the issues concerning significance testing. Dr. Ron Gelaro, of the Naval Research Laboratory, provided the model data used and offered helpful suggestions for improving the study. I would also like to thank Mike McCann and the Naval Postgraduate School Visualization Laboratory for his outstanding work in animating the model data fields. Finally, I thank my wife, Stacey, and my children, Cassidy and Fletcher, for their patience and support.

TABLE OF CONTENTS

I. INTRODUCTION

During the past two decades there has been an increasing amount of research on the tropical atmosphere devoted to low-frequency or intraseasonal oscillations, such as the oscillation detected by Madden and Julian (1971) in tropical Pacific pressures and winds. Madden and Julian (1972) showed that this oscillation, referred to here as the *Madden-Julian oscillation* (MJO), has a period of about 40-50 days, is of global scale, possesses features of an eastward moving wave with zonal wavenumber one, and can be associated with regions of enhanced large-scale convection which oscillate with a similar period. Similar oscillations, with a period of 30-60 days, in the zonal wind and geopotential height, have also been shown to exist in the extratropics (Krishnamurti and Gadgil 1985; Ghil and Mo 1991). These different oscillations have prompted several studies into tropical - extratropical interactions on intraseasonal scales (e.g., Weickmann et al. 1985).

Such long distance relationship are referred to as teleconnections. Bjerknes (1966) provided much of the motivation for the teleconnection studies of the last 25 years. He observed that increased sea surface temperature along the equator in the central and western Pacific, during the 1957-58 winter, was accompanied by strengthened

midlatitude westerlies over the northeast Pacific. As a result, several researchers have examined one aspect of tropical-extratropical interactions, the relationships between tropical heating and higher latitude circulations (e.g., Chang and Lau 1982; Lau et al. 1983; Chang and Lum 1985; Hurrell and Vincent 1990,1991). This has become a topic of great importance, because the possibility of predicting variations in extratropical circulations, due to observed oscillations in tropical heating, could be very useful in improving extended-range midlatitude weather forecasts.

Numerous observational studies have examined how oscillations in tropical convection may cause variations in the local Hadley circulations and influence upper-level extratropical circulations. Chang and Lau (1982), in a composite study of observed monsoonal cold surges over the South China Sea, found that cold surges and increases in tropical convection and divergent outflow occur almost simultaneously. They suggested that the increased tropical convection was responsible for strengthening the local Hadley cell over east Asia, which caused an intensification of the east Asian jet streak. During "break" periods, (periods of weak tropical convection in the west Pacific and sustained southerly surface winds over the South China Sea), there was a weakening of the tropical divergent outflow and a deceleration of the East Asian jet streak. In addition, over the equatorial Indian Ocean, development of upper-level

divergence and strengthening of the jet streak over west Asia was observed. Their results support the idea that tropical convection, through the Coriolis torque acting on divergent tropical outflow, may accelerate extratropical circulations.

In a follow-on study, Lau et al. (1983) investigated short-term interactions between the tropics and midlatitudes using objectively analyzed wind data for December 1978 to February 1979. They showed that fluctuations in the jet can be influenced by changes in eddy activity, as well as by tropical convection. However, in the jet entrance region, upper-level divergent flow in the East Asian Hadley circulation, due to enhanced tropical convection, appears to be the predominant factor responsible for jet acceleration. Downstream of the entrance region, the jet is maintained largely by convergence of eddy momentum flux.

Chang and Lum (1985) used 200mb wind data for December 1983 to February 1984 to examine the transient interaction between the upper-level tropical divergent outflow and the midlatitude jet. Their findings further substantiated the conclusions of Lau et.al. (1983), with significant positive correlations between regions of upper-level tropical divergence and extratropical westerly wind maxima throughout the season. More important was their conclusion, based on three tropical cyclone events, that the intensifications of the midlatitude jet are likely to be the result, rather than the cause, of the tropical-extratropical interaction.

Several other observational studies have examined the MJO to provide further evidence of tropical-extratropical teleconnections. For example, Weickmann et al.(1985), used 28-72 day planetary-scale oscillations of outgoing longwave radiation (OLR) and 250mb streamfunction data, during ten years of northern hemisphere winters, to determine if any statistical evidence existed for links between the tropics and extratropics. The OLR fluctuations were interpreted as fluctuations in large-scale tropical convection. The strongest fluctuations had a 28-72 day period and occurred in the equatorial regions of the Indian and western Pacific oceans. The streamfunction variance showed oscillations with a 28-72 day period over the subtropics of both hemispheres and over the extratropical North Atlantic. Their study also showed that the relationship between regions of inferred large-scale convection in the tropics and extratropical circulation features were statistically significant. Specifically, they found that when the tropical convection was near the dateline, a strengthened jet occurred over the central Pacific, while a weakened central Pacific jet was observed when the tropical convection was further west over Indonesia.

Knutson et al.(1986) used OLR and 250mb zonal wind data from nine northern hemisphere summers to show that the tropical OLR oscillations had the largest variance in the equatorial Indian and western Pacific Oceans. They also found

that an enhanced subtropical jet in the southern (winter) hemisphere at 30°S was well correlated with negative tropical OLR anomalies. Knutson and Weickmann (1987) also examined tropical OLR anomalies, global streamfunction, and velocity potential data at 250mb and 850mb. They found the extratropical "response" to inferred tropical convection in both winter hemispheres to be statistically significant. They also identified patterns in the fluctuations of large-scale tropical and extratropical weather patterns. For example, during the November-April season, the East Asian jet tends to retract toward Asia when positive convection anomalies are present over the equatorial Indian Ocean. Eastward shifts of the convection into the western and central Pacific tend to be accompanied by eastward extensions of the East Asian jet. Similarly, during the May-October season, the shift of convection anomalies from the Indian Ocean and Indian monsoon regions to the tropical western Pacific is followed by a strengthening of the westerlies over southern Australia. However, they found that the extratropical response in the summer hemispheres was not statistically significant.

In a study by Hurrell and Vincent (1990), the relationship between tropical heating, represented by upper tropospheric velocity potential, and subtropical jets was examined for southern hemisphere summer cases. They found the highest positive correlations, between tropical velocity potential and subtropical westerly wind maxima, existed over four distinct

regions: the Indian Ocean between 70°E and 85°E; the western Pacific near 150°E; the central Pacific near the South Pacific Convergence Zone (SPCZ); and a narrow band near the South Atlantic Convergence Zone (SACZ). Very poor correlations were noted whenever upper level convergence was present. They suggested that subtropical westerly maxima can exist at all times, but are particularly enhanced during periods of strong upper level tropical outflow. They also suggested, because of the relatively short latitudinal distances between the maximum tropical outflow and the subtropical westerly flows (about 16°), and the 12-hour data used, that the initial subtropical response could occur in as little as 12 hours.

Hurrell and Vincent (1991), utilized several additional analysis tools to quantitatively examine the extent to which the tropical, diabatically driven upper-level divergent circulations interact with extratropical jets. They partitioned the ageostrophic wind into divergent and rotational components, applied localized Eliassen-Palm flux diagnostics, and examined the complete kinetic energy budget separated into rotational and divergent components. Their findings indicated that the divergent component of the ageostrophic wind accounted for nearly all of the ageostrophic wind in the southern hemisphere summer subtropics. In the northern hemisphere winter, the ageostrophic wind was largely rotational. They therefore suggested that tropical divergent circulations force the local summer subtropical westerlies

much more than the local wintertime jets. In their analysis of the kinetic energy budget, they showed that the generation of divergent kinetic energy and its conversion to rotational kinetic energy were the dominant terms in the summer hemisphere subtropics. Thus, their results support the argument that subtropical westerlies may be maintained by the tropical divergent circulations.

In addition to the observational studies mentioned above, tropical-extratropical interactions have been studied using numerical models. Nogues-Paegle and Mo (1988) used a general circulation model (GCM) to examine the transient response of the southern hemisphere subtropical jet to tropical forcing during the 1979 southern hemisphere winter. Their study focused on circulation changes during an episode of enhanced latent heat release in the tropics and an enhanced subtropical jet stream over Australia. In a 15 day control run, the model reproduced the location of enhanced tropical convection to the northeast of the jet, four days prior to the occurrence of the jet maximum. The model also successfully simulated the strengthening of the 200mb jet. The jet maximum was in good agreement with the observations, although somewhat weaker. Nogues-Paegle and Mo also performed a second run in which tropical heating was suppressed from 90°E to 120°W. This run showed decreased values of the jet over Australia. Based on these results, they offered the following time scales of response of subtropical latitudes to tropical latent heat

release: divergent and ageostrophic circulations react in 1-2 days, impact is felt in the subtropics in 2-4 days, and is fully established in about 6 days. Thus, their work also supports the theory that tropical heating, through local meridional circulations, is linked to accelerations of the extratropical zonal wind.

Sardeshmukh and Hoskins (1988) offered a theoretical explanation of tropical-extratropical interaction based on experiments with a barotropic vorticity model. They noted that the extratropical response to anomalous tropical heating is essentially a problem involving Rossby wave propagation and dispersion in a sheared ambient flow. They showed that vorticity advection by the divergent portion of the horizontal flow is crucial for understanding tropical-extratropical interactions and include this term in their definition of the Rossby wave source. This Rossby wave source was shown to be very asymmetric about the equator, and strongest on the equatorward flanks of the winter subtropical jet, even for symmetric tropical heating. They argued that this explains how the extratropical response can be large in the winter hemisphere, even when the heating occurs entirely in the summer hemisphere, and why the response is considerably larger in observations and in GCM simulations than in simpler models. They concluded that prediction of a specific midlatitude response remains difficult and requires the full complexity of a GCM to simulate the upper level divergence/convergence

divergence/convergence patterns and the zonal variations of the basic state accurately.

The western equatorial Pacific, because of its high sea surface temperatures, strong convection, persistent tropical storms, and large concentrations of heat and moisture, is often seen as the driving source for the global atmospheric circulation (Webster, 1981). Nitta (1987) examined the intraseasonal variations of convection in this area and their impact on extratropical weather. He showed that convection was largely modulated by the MJO and suggested that when large convective regions (2000-3000 km in diameter) occur over the Philippine Sea, Rossby wave trains, related to the enhanced heating, manifest themselves in the midlatitude mean flow and propagate east across the north Pacific to North America in a period of about five days.

The primary motivation for this study comes from the work of Murphree and Gelaro (1992) who, while investigating the North Pacific-North American teleconnections using a GCM, found intraseasonal variations in the extratropical responses to tropical heating. These response variations were clearly related to intraseasonal variations in the strength and location of the midlatitude jets and their associated barotropic instabilities. They speculated that tropical heating may produce extratropical responses through its forcing of the midlatitude jet.

The purpose of this study is to analyze the intraseasonal variations of the midlatitude jets and their relationships with the global tropical heating field. This study uses many of the techniques of previous investigators to examine the relationship between tropical heating and individual midlatitude jets, but it differs in several ways. We focus on the northern hemisphere summer (June - October), while most previous observational and modeling studies focused on the winter hemisphere. This choice was influenced by the Hurrell and Vincent (1991) conclusion that tropical divergent circulations play a much greater role in the direct forcing of local summertime extratropical westerlies than in the forcing of local wintertime jets. We use the spectral analysis techniques described by Weickmann et al. (1985) and others to determine the model's effectiveness at simulating intraseasonal (30-60 day) oscillations in tropical heating and in the extratropical upper-level circulation. We also use composite and cross-correlation techniques to identify the relationships between these fields. Finally, we examine the teleconnections between *individual* midlatitude jets and heating *throughout* the tropics, unlike some previous studies that have tried to identify the global circulation response to individual tropical heatings.

Chapter II discusses the model, the model run, the model output fields, and the analysis procedures used. Chapter III presents the statistical analyses of the model fields. Chapter

IV discusses and interprets the analysis results, presents our conclusions, and proposes areas for future study.

II. MODEL, DATA, and ANALYSIS PROCEDURES

The model used for simulating the northern summer circulation was Version 3.2 of the Navy Operational Global Atmospheric Prediction System (NOGAPS), a global spectral model. NOGAPS is the U. S. Navy's current operational numerical weather prediction model, providing global atmospheric forecasts to operating U.S. military forces around the world, from the Fleet Numerical Oceanography Center (FNOC) in Monterey, California. In order to run the climate simulation, the model's resolution was set at T49 (triangular 49 truncation), corresponding to a 2.5° latitude-longitude transform grid. It has 18 levels in the vertical. Other model features include a high wind spectral filter, which increases model time steps, and the Arakawa-Schubert cumulus parameterization scheme. A more detailed description of NOGAPS is provided by Hogan and Rosmond (1991).

A 120 day run, started from 15 June 1990 conditions, provided the heating and wind data. This model run used fixed northern summer climatological mean sea surface temperatures.

Four primary data sets were utilized in this study. The NOGAPS 200mb u (U200) and v (V200) winds, along with the 200mb streamfunction (Ψ) were used to describe the intraseasonal variations in the midlatitude upper-tropospheric circulation. The OLR field was used to infer tropical convection and

heating. Relatively low (high) OLR values correspond to relatively strong (weak) convection and heating (see Arkin and Ardanuy 1989). The daily 0000 GMT value of each variable was used to construct the data sets used in this study.

Various measures of the extratropical circulation were considered, including the 200mb zonal (U200) and meridional (V200) wind components, the streamfunction (Ψ), and the kinetic energy (KE) fields. We have focused on the KE and Ψ fields because each compactly represents both components of the horizontal flow in a single term. From the extratropical U200 and V200 fields, the kinetic energy at each grid point was calculated as:

$$KE = \frac{(U200^2 + V200^2)}{2}$$

Anomaly fields were calculated by removing the mean and the linear trend of the 120-day time series for each field, at each grid point.

Spectrum analysis techniques utilizing the Fast Fourier Transform (FFT) method were used to obtain spectral representations of the OLR and KE fields. For the 120-day time series, 60 Fourier frequencies, given by $n/120\Delta t$; n = 1,2,..., 60 and Δt = 1 day, were available. The Fourier frequencies corresponding to periods of 30, 40, and 60 days comprised the spectral band of primary interest for this study. Various studies have shown that the 30-60 day spectral

band is an appropriate choice to capture the fluctuations associated with the MJO (e.g., Weickmann et al. 1985, Kiladis and Weickmann 1992). These periods were isolated by simple truncation of all Fourier components outside this spectral band. Due to Gibbs effects, this spectral band is likely to contain variance from bordering frequency bands covering periods ranging from 27 days to 80 days (corresponding to half-band intervals of 1.5 and 4.5 cycles per 120 days). More sophisticated filtering methods were not used, since they would have provided minimal improvements for our relatively short time series.

The net result of removing the time mean, linear trend, and frequencies beyond the intraseasonal band is what we will refer to as a *processed* data set. A processed data set represents the intraseasonal anomaly part of the original data set.

In order to assess the statistical significance of the model fields, red noise spectra were computed at each grid point based on the lag-one autocorrelation coefficient. The ratio of the 30-60 day variance and the total variance was tested at the 99% significance level against the red noise background spectra. The red noise continuum is generally more appropriate for use as a background spectra than the level white noise spectrum, because it takes into account some of the effects of persistence in the data (Gilman et al. 1963).

A detailed description of these techniques is provided in Appendix B.

Composite and cross-correlation techniques were used to identify relationships between tropical OLR and extratropical jets at intraseasonal time scales. The composite technique is based on the occurrence of relative maxima and minima in an extratropical processed KE time series for a specific region. The technique is explained in more detail in Appendix C. Cross-correlations between the processed OLR and regional kinetic energy fields were performed in order to generalize the results of the composite procedure.

Previous studies have focused on tropical heating in a specific area and its relationship to other variables over hemispheric or global domains (e.g., Kiladis and Weickmann, 1992). This study differs by focusing on a specific area in the extratropics and examining the relationships (i.e., the teleconnections) between the KE in that area and the OLR field at *every* tropical grid point.

The following acronyms describe the geographic areas that are referred to often in this study. The latitude and longitude ranges listed for these areas are approximate.

1) WESTERN PACIFIC OCEAN

   WESTPAC (5°N - 25°N, 100°E - 150°E)

2) TROPICAL (30°S - 30°N)

   IO - Indian Ocean (60°E - 100°E)

   WP - western Pacific Ocean (100°E - 160°E)

   CP - central Pacific Ocean (160°E - 140°W)

   EP - eastern Pacific Ocean / Caribbean Sea (140°W - 60°W)

   AT - Atlantic Ocean (60°W - 10°W)

   AF - Africa (10°W - 60°E).

3) EXTRATROPICAL (40°N - 60°N)

   NP - North Pacific (160°E - 125°W)

   NA - North America (110°W - 55°W)

   NAT - North Atlantic (55°W - 5°W)

   EU - Eurasia (35°E - 95°E)

   EA - East Asia (95°E - 160°E)

III. MODEL RESULTS

A. TROPICAL HEATING

Several fields produced by NOGAPS were considered to represent the model's tropical heating. These included cumulus heating (CHT), total vertically-integrated heating (VHT), outgoing longwave radiation (OLR), and velocity potential (χ).

The mean CHT field for the 15 June - 12 October 1990 study period (Fig. 1a) shows relatively localized tropical heating maxima over the western tropical Indian Ocean and the Arabian Sea, the Bay of Bengal, the East China Sea, and the maritime continent. Broader areas of tropical heating appear in the vicinity of the SPCZ and ITCZ (Inter-Tropical Convergence Zone) in the central Pacific, the Caribbean Sea, and the tropical North Atlantic.

As expected, the mean VHT field for the same period (Fig. 1b) shows heating maxima in similar areas although the magnitude and spacial coverage of the heating is slightly increased. Noticeably absent in both the CHT and VHT is any representation of heating over the land masses of southern Asia or tropical South America and Africa.

The mean tropical OLR field for the study period is shown in Figure 1c. Low tropical OLR values ($\leq$ 230 W/m^2) indicate areas of deep convection and intense heating. These areas

include the ITCZ extending across Africa into the south Atlantic; the SPCZ in the central Pacific; central Mexico; the Sargasso Sea; and the Indian monsoon region. High OLR values ($\geq$ 280 W/m^2) observed off the west coasts of North and South America and northern and southern Africa indicate clear sky conditions and relatively little tropospheric heating. Also, for reasons not yet clearly understood, the model produces four distinct cooling centers — in the central Indian Ocean, over Sumatra and the Malaysian peninsula, over Borneo, and over the southern Philippine Islands — where enhanced tropical heating should be expected. The region east of the Philippines (0°-25°N, 130°E-180°E) is another area where low OLR values would be expected during the northern summer but are not apparent in the model's simulation. It appears that NOGAPS has displaced the heating associated with the western and central Pacific ITCZ to the north and the expected maritime continent heating to the south, resulting in a somewhat distorted mean OLR field observed.

Figure 1d shows the mean global velocity potential field (χ) at 200mb for the study period. Negative values of χ indicate regions of upper tropospheric divergence and can be used as a very broad scale indicator of convective activity. A zonal wavenumber one pattern is readily apparent with upper-level divergence present from 60°E-140°W, with a maximum located over the north Pacific at 20°N. Upper-level convergence is present from 140°W-20°E with maxima in the

eastern Pacific and south Atlantic Oceans. This field is in close agreement with the OLR field, in that the relatively wide spacing of the contours in the maritime continent area suggests upper-level convergence and reduced heating. Positive maxima, located off the west coasts of the Americas and Africa, also indicate upper-level convergence and reduced heating, which is in agreement with the high OLR values in similar regions (Fig. 1c).

All four of these fields —— CHT, VHT, OLR and χ, —— provide useful representations of the model's tropical heating. However, OLR was chosen for this study for several reasons. First, observed OLR fields derived from twice-daily measurements from polar-orbiting satellites provide a method of direct comparison to observations not available with the other heating fields. Second, OLR has been widely used to represent tropical convection which allows direct comparisons with previous studies (e.g., Knutson et al. 1986). Finally, the OLR field provides a more plausible representation than the CHT and VHT fields do of heating over the large tropical land areas (i.e., Southeast Asia, South America, and Africa).

This paper will focus on OLR fluctuations in the tropical latitudes from 30°S-30°N. Areas with a low (high) OLR, or a negative (positive) OLR anomaly, will be assumed to be areas with relatively large (small) tropospheric heating, or heating that is enhanced (reduced) with respect to the mean for the 120-day period.

As described in Chapter II, the OLR field was linearly detrended, and a 30-60 day band pass filter was applied, resulting in a processed OLR (POLR) anomaly field. The time series of the POLR field for a tropical western Pacific region (WESTPAC) (5°N-25°N, 100°E-150°E) retains only the intraseasonal signal of the original OLR time series (Fig. 2). Figure 3 shows the periodogram for the unprocessed OLR time series, shown in Figure 2, for the WESTPAC region. The signal in the 30-60 day period range (2-4 cycles per 120 days) is clearly the dominant signal for the WESTPAC area, accounting for nearly 30% of the total variance, and is generally representative of other tropical areas. Area-averaged periodograms for the Indian Ocean, and African regions (not shown) exhibit slightly stronger signals, while the eastern Pacific region (not shown) shows a slightly weaker signal, for the 30-60 day spectral band.

Although the mean OLR field shows interesting results, how the OLR field changes during the model run is more useful to determine the character of the 30-60 day tropical oscillation and its relationship to the extratropics. Figure 4a shows the model's OLR variance (2-120 day period) and Figure 4b shows the model's POLR variance (30-60 day period). Several areas of high variance are similar in both fields. Note though that the POLR field has distinct areas of high variance over the Southeast Asian land mass and tropical Africa. The major areas of high variance in the POLR field are southern Asia,

north of the equator in the tropical Indian and western Pacific Oceans, east of New Guinea in the SPCZ region, and over equatorial Africa. Regions of low OLR variability are seen off the west coasts of the Americas and Africa, similar to the high OLR areas of Figure 1c. These areas correspond to regions of infrequent deep convection, strong subsidence, high sea-level pressures, and low sea surface temperatures.

The ratio between the 30-60 day variance and the total variance was tested at the 99% significance level against the percent red noise background spectra in order to determine areas of statistically significant 30-60 day OLR variability (see Appendix B). The shaded regions in Figure 4c indicate areas of significant 30-60 day OLR variance. Major areas of significance are in the tropical Indian and western Pacific oceans, southern Asia, the central Pacific, the southeast Pacific off the west coast of South America, continental South America, the Caribbean and Sargasso Seas, the southeast Atlantic and west Africa, and northeast Africa and the Arabian peninsula. In general, most areas that showed high 30-60 day variance were significant when tested against a background red noise continuum at the 99% significance level.

Figure 4 is comparable to a figure from Knutson et al. (1986, Figure 1) which is reproduced in Figure 5. Comparison of the total variance maps (their Fig. 5b and our Fig. 4a) and filtered variance maps (their Fig 5c and our Fig. 4b) shows good general agreement. They found the largest total and

intraseasonal (28-72 day period) variance in OLR over the Indian monsoon region, the western equatorial Pacific, and the eastern tropical Pacific west of Central America, which is similar to our results, with the following exceptions:

- our results show a much stronger intraseasonal variance over equatorial Africa
- the variance in our results is 5-10 times greater in magnitude

The differences in the locations of the high and low variance areas are due in part to the sampling method. Our OLR data is based on a once-daily sampling at 0000 GMT, while their OLR data is a daily average derived from twice-daily satellite measurements. Their data is then grouped into non-overlapping five-day averages for each year and then averaged over the nine summers of their study period. This averaging reduces their variances and directly affects the results shown on their significance maps (their Fig. 5d). The much larger area of significance in the model fields probably results from the model OLR's high variance, the absence of any averaging of the model OLR, and the application of the 30-60 day filter to the relatively short model time series (120 days).

In order to determine the periodicity and propagation of the OLR oscillations, the POLR anomaly field is displayed in a time versus longitude format for the 5°S - 5°N latitude band (Fig. 6). The dominant features are the eastward propagation of the POLR anomalies in the Indian Ocean and equatorial

western Pacific regions (60°E - 160°E) and the standing anomalies in the African region (20°W - 50°E). An example of eastward propagation is the strong negative anomaly in the Indian Ocean region around 24 June that moves to the western Pacific region by 20 July at about 3.5 m/s. Two similar oscillations are also seen in the same area over 24 July - 13 August and 7 - 22 September. Propagation speeds vary from 3-7 m/s, which agrees with previous studies of the northern summer (Knutson et al., 1986). Note that the OLR in the equatorial Indian and western Pacific Ocean region oscillates with a period of about 40 days. The standing feature over Africa appears to have a period of about 30 days, with maximum negative anomalies occurring at 4 July, 3 August, 2 September, and 2 October. Other prominent features appear in the central and eastern Pacific and Atlantic Oceans, but the propagation of these features is generally less distinct than in the Indian and western Pacific Oceans.

B. EXTRATROPICAL WINDS & KINETIC ENERGY

The mean 200mb vector wind field for the study period is shown in Figure 7a. The strongest westerly winds occur in the midlatitude jets of the southern hemisphere, from 30°S-60°S, and the northern hemisphere from 40°N-60°N. There is a strong tropical easterly jet extending from the western Pacific monsoon region across the Indian Ocean to Africa. As previously discussed, this study focuses on the northern

hemisphere extratropical circulation. Figure 7b shows the mean zonal component (U200) of the 200mb wind for the study period. The northern hemisphere midlatitude jet streams can be seen, with jet cores occurring over northern Asia and extending into the northern Pacific, and over North America and extending into the North Atlantic. Subtropical jets occur in the northeast Pacific and western U. S., and over northern Africa and the Mediterranean Sea. The tropical easterly jet extends from the west Pacific monsoon region across the African continent, with its core over East Africa.

As discussed in Chapter II, this study will utilize kinetic energy (KE) to represent the extratropical circulation. The mean KE field for the study period is shown in Figure 7c. Note that the KE field is very similar to the U200 field, indicating that most of the kinetic energy is contained in the zonal wind.

In order to emphasize the tropical - extratropical interaction on the intraseasonal (30-60 day) time scale, the KE field was detrended and band pass filtered in the same way as the OLR field (see Chap. II for details). The North Pacific (NP) area-averaged time series for the original KE field and for the processed KE field is shown in Figure 8. The processed KE field clearly shows the intraseasonal signal of the original KE field. Figure 9, the periodogram for the NP region, shows a strong signal in the 30-60 day period range, which accounts for over 40% of the total variance. The

strength of the signal in the 30-60 day spectral band for this region is typical of the majority of the 40°N - 60°N latitude band.

Positive (negative) PKE anomalies are used to infer midlatitude jets that are stronger (weaker) than the 120-day mean. This PKE field and the POLR field are used in the composite and cross-correlation analyses that are presented in the next section.

The variance maps for the unprocessed KE field and for the PKE field are shown in Figure 10. The northern hemisphere areas with the largest variance are similar for both fields and can be separated into five distinct regions. These regions are in the: North Pacific (NP), North American (NA), North Atlantic (NAT), Eurasian (EU), and East Asian (EA) areas. These high variance areas are outlined by the boxes shown in Figure 10b. The grid point values of the PKE in each of these boxes are averaged together at each time step to produce five area-average regional time series.

The EA, NA, and EU high variance regions generally overlie the jet core regions shown in Figure 7b. The high variance in these areas can be attributed primarily to changes in jet strength. The NP and NAT high variance regions overlie jet extension areas where the high variance is due to changes in jet strength, location, and direction. We have focused our study on the NP and NAT jets because of the importance of

these jets in extended range forecasting for North America and Europe.

The statistical significance of the PKE field was tested in the same way described for the POLR field (see Appendix B). The shaded regions of Figure 10c indicate areas of significant 30-60 day PKE variability. In the northern hemisphere, the five areas of high variance in the PKE field —— NP, NA, AT, EU, and EA —— all remain significant at the 99% significance level.

Knutson et.al. (1986) used the 250mb zonal wind field (U250), to examine the upper-level circulation. Their Figure 2, reproduced in Figure 11, shows the variance of their zonal wind field and is somewhat analogous to our Figure 10. Their streamfunction had the largest total and intraseasonal (28-72 day period) variance in the climatological jet streams (their Fig. 11b and c). This result is in general agreement with our results (Fig. 10a and b).

As previously discussed, the averaging done by Knutson et al. (1986) probably has reduced their U250 variance and areas of significance. Due in part to the model's high KE variance and the filtering of the relatively short time series (120 days), we obtained an intraseasonal variance that is significant over a much larger global area than shown by Knutson et al. (1986) (compare their Fig. 11d with our Fig. 10c). We also show significance in the extratropical KE, but

not in the tropical KE, which is the opposite of what they found.

A time-longitude diagram for the midlatitude PKE anomaly field is shown in Figure 12. The dominant feature is the eastward propagation of the PKE anomalies in the longitudes from about 20°E - 60°W. One example is the positive PKE anomaly in the European area on about 13 August that propagates eastward to the North Atlantic by 22 September. The oscillation of the PKE anomalies is also clear. For example, the positive PKE anomaly in the east Asian area on about 19 July changes to a negative anomaly around 8 August, and back to a positive anomaly by 7 September, indicating a period of about 40 days. Some of the PKE oscillations exhibit distinct phase relationships. For example, the centers of maximum variability in the east Asian, North Pacific, and North American regions oscillate in phase with each other, but out of phase with the North Atlantic and Eurasian regions. The speed of the oscillation in the EA/NP/NA regions appears to be approximately 18°/day or 15 m/s. There also appears to be a westward propagation in the North Atlantic / European area (60°W- 20°E).

In this study we attempt to clarify the intraseasonal relationships between tropical heating and extratropical circulation. Figure 13 shows the intraseasonal variation of the NP PKE and tropical western Pacific POLR, with the POLR leading the PKE by about 14 days. The strong correlation

between the two series indicates that tropical heating in specific areas may force fluctuations in specific and distant midlatitude jets. To explore this possibility, we have performed composite and correlation analyses which are presented in the next section.

C. COMPOSITE AND CORRELATION ANALYSES OF EXTRATROPICAL KINETIC ENERGY AND TROPICAL OUTGOING LONGWAVE RADIATION

1. North Pacific Jet Region

a. Jet - Jet Composite Relationships

As previously discussed, the variance map of the PKE field (Fig. 10b) showed a distinct core region in the North Pacific. An area-averaged time-series of the PKE anomaly field was calculated for this region (Fig. 14). As discussed in Section B, the maxima (minima) in the PKE anomaly field represent jet maxima (minima). Figure 14 shows that for the NP region, the jet maxima (minima) occurred on 3 August and 11 September (28 June, 23 August, and 28 September).

In order to determine the relationship between the NP jet and other midlatitude jets, composite maps were produced by averaging the PKE anomaly values at each grid point for all times when there was a maximum (minimum) in the NP jet. This averaging was also done for each of the 10 days preceding and following the maximum (minimum) (see Appendix C for details).

Figures 15 and 16 show the global composite PKE anomaly field at several times before, during, and after composite NP jet maximum and minimum, respectively. Note that prior to the composite NP jet maximum (Fig. 15a-b), a composite jet maximum is located to the west, in the East Asian region, and that in the period following the NP jet maximum (Fig 15d-e), the relative jet maxima has begum to build up to the east, over the North American region. Similarly, during the period preceding the NP jet minimum (Fig. 16a-b), an eastward propagation from East Asia to North America of a relative jet minimum occurs. Also evident is the relationship described previously using the time-longitude diagram (Fig. 12); namely that when a maximum (minimum) is present in the NP region, relatively strong positive (negative) PKE anomalies are also present in the EA and NA regions, and weak negative (positive) anomalies occur in the AT and EU regions.

Also of interest is the variation of the composite PKE anomaly field in the southern hemisphere midlatitudes. Although Figures 15 and 16 are based on the maximum and minimum in the NP composite PKE, it appears that similar jet - jet relationships are present in the southern hemisphere. However, we will not pursue these relationships in this study.

b. Jet - OLR Composite Relationships

Composite maps of the tropical (30°S-30°N) POLR field, for the 21 day period (± 10 days) surrounding the composite NP jet maximum (minimum), were constructed using the same procedure described previously. As discussed in Section A, negative (positive) POLR anomalies are associated with areas of enhanced (reduced) tropical heating.

Figure 17 shows the negative and positive composite POLR anomaly fields for ten and five days prior to, during, and for five and ten days following the composite NP jet maximum.

Ten days prior to the NP jet maximum (Fig. 17a), enhanced heating is scattered throughout the Pacific and southern Indian Ocean. Enhanced cooling is present over most of the western Pacific, Indian and the tropical Atlantic Oceans.

Five days prior to the NP jet maximum (Fig. 17b), there are three major areas of enhanced heating: 1) over and to the east and southeast of the Philippines; 2) over western equatorial Africa and the tropical east Atlantic; 3) over South America along 20°S and extending into the southeastern Pacific. The corresponding positive composite POLR anomaly field shows enhanced cooling in three major areas: 1) over the Indian Ocean; 2) east of New Guinea extending southeast along the SPCZ; 3) over the northwest Atlantic.

When the composite NP jet is at a maximum (Fig. 17c), the heating anomalies remain strong over and to the east of the Philippines, have started to strengthen over southeast Asia, north of Australia, near the dateline in the central Pacific, and the equatorial Atlantic, and have diminished over continental South America. The corresponding cooling anomalies have intensified in the southern Indian Ocean, have started to develop in the south-central and eastern Pacific, and have diminished east of New Guinea.

Five days after the NP jet maximum (Fig. 17d), the NA jet maximum has begun to strengthen, and the tropical heating anomaly field shows a southwestward shift of the heating from the Philippines area to the area east and northeast of New Guinea. The heating anomalies have remained strong over Southeast Asia and north of Australia, and have strengthened over India, the central Pacific, and the South Atlantic. During this period, the cooling anomalies over the southern Indian and southcentral Pacific oceans have diminished while over the eastern Pacific they have intensified.

Ten days after the NP jet maximum (Fig. 17e), the heating anomalies have strengthened over the Indian Ocean, east of New Guinea and extending southeast along the SPCZ, and over the northwest Atlantic. The corresponding cooling anomalies have intensified over and to the east and southeast of the Philippines, and over equatorial West Africa extending

into the tropical eastern Atlantic. Note that the pattern of POLR anomalies, five days prior to the NP jet maximum, is nearly opposite to the POLR pattern ten days after the NP jet maximum. Areas of enhanced (reduced) heating five days prior to the jet maxima, such as the WP and AF (IO) regions, have evolved into areas of reduced (enhanced) heating ten days after the NP jet maximum.

Also of interest are the relationships between tropical POLR anomalies and the NP jet before, during, and after the composite NP jet is at a minimum. Figure 18 shows the negative and positive POLR anomaly fields for ten and five days before, during, and for five and ten days after the composite NP jet minimum. Comparison of analogous panels of Figures 17 and 18 reveals that the major regions of *enhanced* tropical heating associated with a NP jet maximum are very similar to the regions of *reduced* tropical heating associated with a NP jet minimum. Similarly, regions of reduced tropical heating associated with NP jet maxima are also very similar to the regions of enhanced heating for the period surrounding a NP jet minimum.

c. KE - OLR Cross-Correlations

In order to supplement the results obtained from the composite analysis, a cross-correlation technique was used to determine statistical relationships between the NP jet and tropical heating.

The correlation coefficients between the area-averaged PKE anomaly time series for the NP region (Fig. 14) and the time series of POLR anomalies at every tropical gridpoint were calculated for lags of ±10 days. *Positive lags* indicate that the tropical POLR anomaly (and, thus, the heating or cooling anomaly) leads the extratropical jet, while *negative lags* indicate that the tropical POLR anomaly lags the jet. To focus on enhanced tropical heating and cooling, only correlation coefficients ≥ ±0.4 for the latitude band from 30°S-30°N are considered.

The correlation analyses assume that there is a nearly linear relationship between OLR and the extratropical jet. Kiladis and Weickmann (1992) contend that this assumption is valid to the extent that OLR anomalies are linearly related to tropical heating anomalies, and to the extent that linear dynamics explains the response to tropical heating. But, as they point out, non-linear interactions may be important components of the response to tropical heating.

For a linear relationship, *negative correlations* occur for two specific OLR - jet relationships:

1) enhanced tropical heating (negative OLR anomaly) associated with a strong jet;

2) reduced tropical heating (positive OLR anomaly) associated with a weak jet.

Similarly, *positive correlations* occur for two relationships:

1) enhanced tropical heating (negative OLR anomaly) associated with a weak jet;

2) reduced tropical heating (positive OLR anomaly) associated with a strong jet.

Figure 19 shows the cross-correlations between the NP PKE anomalies and the tropical POLR anomalies for lags of +10, +5, 0, -5, and -10 days. Note the similarities between Figures 17 and 18 and Figure 19. That is, the negative and positive correlation patterns, at lags from +10 to -10 days (Fig. 19a-e), are very similar to the general patterns of positive and negative POLR anomalies associated with the NP jet, ten and five days before, during, and five and ten days after a the composite NP jet maximum (Fig. 17a-e). Also, the general pattern is opposite to the pattern shown, for the ±10 days surrounding a composite NP jet minimum (Fig. 18a-e). Since only correlations with magnitudes greater than or equal to ±0.4 are plotted, the areas of strong correlations are slightly smaller than the analogous composite heating and cooling areas.

Also, as was seen in the composite maps, some of the major correlation patterns at a lag of -10 days (Fig. 19e) are similar to, but opposite in sign, to the patterns at a lag of +5 days (Fig. 19b). For example, the areas of strong positive correlations at a lag of +5 days —— the Indian Ocean, the SPCZ, the eastern Pacific, and the north and south Atlantic —— are areas of strong negative correlations at a

lag of -10 days. Similarly, major regions of strong negative correlations at a lag of +5 days —— such as the western Pacific, southern South America, and equatorial Africa extending into the eastern Atlantic —— are regions of strong positive correlations at a -10 lag.

Similar correlation analyses performed with the *unprocessed* (original) OLR and KE fields (not shown) showed very similar (though weaker) results to those obtained with the *processed* fields. Thus, the basic patterns seen in the composite and correlation figures can be seen *even without filtering*. Therefore, the filtering process only enhances the strong intraseasonal signal present in the original OLR and KE fields.

d. Summary

As a result of the close agreement between the composite and correlation analysis results, a life-cycle of the tropical OLR and NP jet relationships can be described. Figure 20 schematically shows the NP PKE anomaly field and corresponding POLR distribution at eight times in the NP jet cycle. Because we are considering 30-60 day oscillations of the OLR and KE, this life-cycle has a period of about 30-60 days. Thus, the eight stages in Figure 20 are separated by about four to eight days (i.e., about six days). The acronyms presented at the end of Chapter II will be used in describing Figure 20.

It can be seen that in Stages 1 and 2 of the cycle, about six days before and during a NP jet maximum (Fig. 20a-b), enhanced heating is dominant in the WP, CP, and AF regions, while cooling is present in the IO region. As the NP jet goes through the transition from maximum to minimum, in Stages 3 and 4, about six and twelve days after the NP jet maximum (Fig. 20c-d), the IO, WP, and AF regions are also going through transition periods, while enhanced heating is present in the AT region and enhanced cooling in the EP region. About six days before and during a NP jet minimum, in Stages 5 and 6 (Fig. 20e-f), the general pattern of Stages 1 and 2 has been reversed with enhanced cooling in the WP, CP, and AF regions, and enhanced heating in the IO region. As the NP jet transitions back from minimum to maximum, in Stages 7 and 8, about six and twelve days after the jet minimum (Fig. 20g-h), the IO, WP, CP, EP, and AT regions are also in transition or have already evolved into their Stage 1 patterns. Only the AF region is dominated by enhanced heating throughout this transition period. To complete the cycle, the enhanced heating returns to the WP, and AF regions, while cooling develops in the IO region, which lends to the return of Stage 1.

Note the phase relationships in Figure 20:

- When the NP jet is at a maximum, the heating anomalies in the WP, CP, and AT regions are in phase with each other and out of phase with the heating anomalies in the IO and EP regions;

- When the NP jet is at a minimum, the same phase relationships exist, with the exception of the anomalies in the AT and AF regions, which are in transition;
- The heating anomaly in the CP region appears to lag the WP anomaly by one stage.

Table 1 summarizes the general positive and negative POLR anomaly pattern observed during the eight stage life-cycle of the NP jet. Areas dominated by positive POLR (cooling) anomalies are indicated by "**C**", areas dominated by negative POLR (heating) anomalies are indicated by "**H**", and areas with no clear dominance or in transition are indicated by "**T**".

2. North Atlantic Jet Region

The North Atlantic region (NAT) also showed a distinct area of high variance in the PKE field (Fig. 10b). As discussed in Section B, this region is similar to the NP region, in that it is also a jet extension area, with high variance due to changes in jet core strength, location, and direction. The analysis techniques used to study the NP jet region were also applied to the NAT jet region.

From the time series for the NAT region, relative jet maxima (minima) were found to occur on 12 July, 30 August, and 8 October (27 June, 29 July, and 20 September). These maxima (minima) were used to construct a composite NAT PKE anomaly field for the period ten and five days before, during, and five and ten days after a composite NAT jet maxima (minima).

Composite maps of the tropical (30°S-30°N) POLR field, for the 21 day period (± 10 days) surrounding the NAT jet maxima (minima), were also constructed using the procedure described in Appendix C. The cross-correlation technique was also used to supplement and verify the results obtained from the composite analysis.

As in the NP jet analysis, close agreement was found between the composite and correlation analysis results. Therefore, a schematic eight-stage life-cycle of the tropical OLR and NAT jet relationship was constructed (Figure 21).

In Stage 1, about six days before a NAT jet maximum (Fig. 21a), enhanced heating is dominant in the EP, and AF regions, while cooling is present in the CP region. The IO, WP, and AT regions are in transition during this stage. During the NAT jet maximum and for about six days after, Stages 2 and 3 (Fig. 21b-c), enhanced heating is present in the WP and EP regions, while enhanced cooling is present in the IO and AT regions. As the NAT jet transitions from maximum to minimum, in Stage 4, the WP, EP, and AT regions are also going through transition periods (Fig. 21d), while enhanced heating is present in the CP region and enhanced cooling in the IO and AF regions. About six days before and during a NAT jet minimum, in Stages 5 and 6 (Fig. 21e-f), the general pattern of the early stages has been reversed, with enhanced cooling in the WP, EP, and AF regions, and enhanced heating in the IO region. As the jet transitions back from

minimum to maximum, about six and twelve days after the jet minimum, in Stages 7 and 8 (Fig. 21g-h), the WP and EP regions are also in transition or have already evolved into their Stage 1 patterns. The IO and AF regions are dominated by enhanced heating and the CP region is dominated by enhanced cooling throughout this transition period.

As in the NP jet analysis, several phase relationships are apparent in Figure 21:

- When the NAT jet is at a maximum, the heating anomalies in the WP, EP, and AF regions are in phase with each other and out of phase with those in the IO and AT regions, while the CP region is in transition (from positive to negative anomalies);
- When the NAT jet is at a minimum, the heating anomalies in the WP, CP, and EP regions are in phase with each other and out of phase with the heating anomalies in the IO region, while the AT and AF regions are in transition (from positive to negative).

Table 2 summarizes the general positive and negative POLR anomaly pattern observed during the eight stage life-cycle of the NAT jet.

D. STREAMFUNCTION AND VECTOR WIND COMPOSITE RELATIONSHIPS

As discussed in Chapter II, the kinetic energy field was chosen to represent the midlatitude jets for several reasons. However, kinetic energy cannot indicate wind direction and gives a poor indication of large-scale eddy patterns. Therefore, the Ψ and vector wind fields were used to gain a clearer understanding of the flow directions and speeds within

different parts of the midlatitude jets and their relationships to the global tropical OLR field.

For the NP jet region, Ψ and vector wind composite anomaly fields were constructed in the same way described for the PKE field (see Appendix C).

Figure 22 shows that, during the composite NP jet maximum, a zonal wavenumber five pattern is present in the extratropics (40°N - 70°N). Also, a strong anticyclone is located in the northeastern Pacific, with a cyclones located to the west and northeast. This pattern corresponds to strong anomalous southwesterly flow in the western half of the NP box, and strong anomalous northwesterly flow in the eastern half, crossing into North America (Fig. 23).

When the NP jet is at a minimum (Fig. 24), this pattern is reversed, with a cyclone in the northeastern Pacific, and with an anticyclone to the north. Figure 25 shows the winds associated with the NP jet minimum. Northeasterly winds dominate the NP box, producing southwesterly flow across the North American west coast.

Similar composite maps were constructed for periods surrounding the composite NAT jet maximum and minimum. Figure 26 shows a strong anticyclone in the North Atlantic and a strong cyclone over the Iceland region when the NAT jet is at a maximum. This combination is responsible for producing the maximum in kinetic energy and the strong anomalous west-northwesterly flow shown crossing into Europe (Fig 27).

As seen in the NP case, an opposite pattern occurs when the NAT jet is at a minimum. Figure 28 shows the Ψ composite anomaly field associated with a NAT jet minimum. Here, a cyclone is present in the north Atlantic, with anticyclonic flow to the north. Strong anomalous east-southeasterly winds are observed over much of the north Atlantic (Fig. 29).

The Ψ composite anomaly field during a maximum in the NP jet (Fig. 22) shows a Rossby wave pattern similar to that described by Nitta (1987) and Harr (1993). Note that Figure 22 represents a period of relatively high (low) heating over the tropical western Pacific (Indian Ocean) (Fig. 17b-c). The Pacific heating corresponds to the heating examined by Nitta (1987). The Indian-Pacific heating dipole corresponds to the heating anomalies studied by Harr (1993). The large-scale extratropical eddy patterns can be useful in determining the mechanisms, such as Rossby wave propagation, that may be causing the circulation anomalies, and their relationship to the tropical heating. Rossby waves are an important component of the large-scale dynamic processes that may be responsible for transporting a tropical heating signal to the midlatitudes (Tribbia 1991, Murphree and Gelaro 1992). Unfortunately, an examination of these dynamic processes is beyond the scope of this study.

E. SUMMARY

The variance of the midlatitude kinetic energy field was used as a basis for investigating specific northern midlatitude jets and their relationships to the global tropical heating field. Detrended and band pass filtered KE data showed five distinct areas of high variance. Two of these areas, the North Pacific and North Atlantic, corresponded to jet extension regions.

The KE in these areas was compared to the tropical OLR field at times surrounding composite jet maximums and minimums. In the NP region, the strength of the composite jet appears to be related to the tropical heating in the western and central Pacific and in Africa. Before and during the composite jet maximum, these tropical regions are dominated by enhanced heating, while before and during the composite jet minimum they are dominated by reduced heating.

A similar relationship was observed for the NAT jet. Before and during the composite NAT jet maximum, the western and eastern Pacific are dominated by enhanced heating, while before and during the composite jet minimum they are dominated by reduced heating.

The general tropical heating and extratropical jet relationships presented in Figures 20 and 21 are encouraging and suggest that general tropical heating - midlatitude jet relationships may exist.

IV. DISCUSSION

A. INTERPRETATION OF RESULTS

In this study, we have explored the relationships between tropical heating and individual extratropical jets using a variety of techniques. This study is unique, in that these relationships are investigated from the perspective of *individual extratropical areas of high kinetic energy variance*. In previous studies, the focus has been on specific tropical areas with high heating variance or specific tropical heating events.

Spectral analyses of both the OLR and KE data sets revealed that the model produced a strong intraseasonal (30-60 day) signal in both fields. This strong intraseasonal signal was responsible for the large OLR and KE variances observed in Figures 4b and 10b, respectively. The presence of the 30-60 day tropical oscillation has been well documented in several observational studies (Madden and Julian 1971, 1972; Weickmann et al. 1985; Knutson et al. 1986; Knutson and Weickmann 1987; Kiladis and Weickmann 1992). Generally, the strength of the signal in the summer hemisphere is considerably weaker than simulated in this model run (Slingo and Madden 1991). The strength of this model's intraseasonal signal was critical for

obtaining the clear indications of tropical forcing of the midlatitude jets found in this study.

Analyzing the tropical OLR field with the use of time-longitude diagrams showed that the model also simulated the MJO reasonably well (Fig. 6). Eastward propagation of tropical convection was evident in the Indian Ocean - western Pacific regions, with a propagation speed (3 - 7 m/s) that is consistent with observations (Knutson et al., 1986). However, previous studies of the MJO using GCM simulations, have had a common inability to produce slow enough phase speeds, with periods of about 25 days typical of the simulated oscillations (Lau et al. 1988; Slingo and Madden 1991). This suggests that NOGAPS may be a particularly useful GCM for studying intraseasonal processes.

The east to west propagation of the intraseasonal KE anomalies, from Eurasia to the North Atlantic, was also very clear throughout most of the midlatitudes, as shown by the time-longitude diagram (Fig. 12). There is, however, an apparent disconnect of the jets in the Atlantic region, where the North American jet and the African extension of the Eurasian jet have a large latitudinal separation. Composite analyses of extratropical KE —— for times before, during, and after relative maxima or minima in the KE for a specific area —— also show the eastward propagation of the intraseasonal KE signal (Figs. 15 and 16). Thus, these results suggest that various jets may be linked to each other

through this slow energy transfer and may be an important mechanism for transporting tropical signals over very long distances.

Composite analyses were also used to identify global tropical heating patterns. Figures 17 and 18 showed that enhanced (reduced) tropical heating at specific locations was associated with the strengthening (weakening) of specific midlatitude jets about a week after the enhanced (reduced) tropical heating. This suggests that tropical heating does produce identifiable responses in the extratropical circulation. These results are consistent with previous modeling studies that found the extratropical response to enhanced tropical heating may establish itself in about a week (e.g., Nogues-Paegle and Mo 1988). The composite results were also supplemented by the results of the cross-correlations between a single area-averaged extratropical KE time series and the OLR time series for all tropical grid points. Both of these techniques produced similar results, thereby giving a measure of self-verification.

When the results of the jet-jet composite relationships and the results of the jet-OLR composite and correlation relationships are looked at in more detail, a new view of tropical - extratropical teleconnections becomes apparent. Because tropical heating and cooling seem to force the jets at preferred locations, and because the jets seem to be well connected, it appears that the jets are an important pathway

for transporting tropical signals. For example, the tropical heating (cooling) in the western Pacific (Indian Ocean) region appears to force the East Asian and North Pacific jets, which then transfer the signal across North America and into the North Atlantic. This idea is supported by the strong negative (positive) correlations of the North Atlantic jet with western Pacific (Indian Ocean) OLR. These correlations (not shown) suggest that the North Atlantic jet may be more influenced by convection in the relatively remote western Pacific and Indian Ocean regions than by much closer convection in tropical South America and the tropical Atlantic Ocean.

The North Atlantic jet does show, however, a good correlation with convection in the eastern Pacific. This convection may be related to the convection signal that previously propagated through the western and central Pacific and led to the strengthening of the North Pacific jet. Thus, as shown in a simple schematic diagram (Fig. 30), the North Atlantic jet may be driven by both:

1) energy propagating into the region from Asia and the North Pacific;

2) energy released in tropical eastern Pacific convective systems.

The more direct response pathway from the tropical eastern Pacific shown in Figure 30 is similar to the energy propagation path shown by Murphree and Gelaro (1992). However, Figure 30 is different in suggesting that more than one

tropical heating region may influence a specific jet, and that remote heating regions may send their signal through a midlatitude jet pathway.

The composite technique was also applied to the model's Ψ and vector wind fields to get a clearer picture of the large-scale circulation features present at times surrounding anomalous PKE maxima and minima, and the relationship of these features to global tropical heating anomalies. From the Ψ anomaly field, a clear wave pattern in the northern hemisphere (Fig. 22) emerges and gives indications of the mechanisms by which energy is transferred from the tropics to the extratropics. The wave pattern in the Ψ field is similar to those seen in previous observational and modeling studies (Nitta 1987; Murphree and Gelaro 1992; Harr 1993; Miller 1993). This wave pattern results in an enhanced ridge - trough - ridge system that develops over North America approximately one week after enhanced heating in the western and central Pacific.

These results offer some practical insight into problems associated with dynamic extended range forecasting (DERF). They suggest that accurate detailed simulations of the global tropical heating field and how it varies are essential for improvements in DERF. It has been shown that when the intraseasonal oscillation was well represented in the tropics of the European Center for Medium Range Weather Forecasting

(ECMWF) model, medium range forecast skill in the extratropics was improved (Ferranti et al. 1990).

B. LIMITATIONS AND PROPOSED AREAS FOR FUTURE STUDY

The model's mean OLR (Fig. 1c) showed irregularities in the heating distribution of the tropical eastern Indian Ocean, the maritime continent, and the tropical western Pacific regions. Also, as previously discussed, when the 120-day mean, variance, and significance diagrams for the OLR and KE fields were compared to similar diagrams from the observational study of Knutson et al. (1986), several discrepancies were noted. This leads us to question exactly how well NOGAPS simulates the real tropical heating field, and therefore, it would be useful to apply the analyses used in this study to global analyses and other model data sets.

This study was limited by several factors. Thus, the results, although encouraging, need to be supported by future studies which address some of these limitations. For example, the relatively short, single-season, time series used cannot assure that the results obtained are representative of a typical northern summer. Therefore, longer, multi-year, time series need to be examined. Also, the sampling method used in this study (daily at 0000 GMT) is probably not the optimum method; a daily average may be more suitable. Finally, a study of the tropical heating - extratropical jet relationships during the northern winter, when the jet is much

closer to the tropical heat source, would be useful to determine the seasonality of these relationships.

The application of a 30-60 day band pass filter to a relatively short time series necessarily constrains the time series to an oscillation with a period at about the midpoint of the band pass window (in this case about a 45-day period). This results in the distinct cyclic behavior found in the PKE and POLR composites (e.g., Figs. 15 - 18). The filtering of the short times series also led to relatively strong KE-OLR correlations (e.g., Fig. 19). For this reason, the magnitudes of the correlation coefficients were not emphasized. However, the similar, although weaker, correlations found using the original unprocessed data, and the similarity of the composite and correlation analyses, suggests that the filtering process served only to enhance the strong intraseasonal signal present in the raw data. To verify this hypothesis, the significance of the KE-OLR correlations should be tested. Kiladis and Weickmann (1992) describe a technique to assess statistical significance using Monte Carlo simulations which accounts for the temporal and spatial autocorrelation of the variables. Such a procedure should certainly be applied when longer time series are used to test the results of this study. In addition, the data should be band passed at shorter periods to examine the teleconnections at higher frequencies.

The composite technique used in this study was useful for determining the jet-jet and jet-OLR relationships at times

surrounding relative maxima and minima. But more sophisticated cluster analysis techniques are available (Harr 1993) and should be used in future studies to gain a clearer understanding of these relationships not only at times of relative maxima and minima, but throughout the time series.

Finally, future studies should examine the dynamical processes that lie behind the tropical heating - midlatitude jet relationships identified in this work. Some new dynamical problems to address are: 1) the different roles played by simultaneous heating and cooling anomalies; and 2) the processes by which the jets interact with each other.

C. CONCLUSIONS

On the whole, these results support our original hypothesis that intraseasonal oscillations in tropical heating have a direct impact on midlatitude circulations, particularly in jet regions. The results have also led to a new hypothesis on the role of the jets in transporting the tropical heating signal.

The strongest correlations between the North Pacific and North Atlantic jets and the global tropical heating field occur when heating anomalies, in specific areas, lead the jets by about one week. This suggests that, in these situations, the tropical heating forces the extratropical circulation anomalies, rather than vice versa.

For the North Pacific jet, strong flow anomalies occur during and after periods of positive heating anomalies in the tropical western and central Pacific and Africa, and negative heating anomalies in the Indian Ocean. Conversely, these heating anomalies are reversed when flow in the North Pacific is weak.

For the North Atlantic jet, strong anomalous flow occurs during and after periods of positive heating anomalies in the tropical western and eastern Pacific and Africa, and negative heating anomalies in the tropical Indian and Atlantic Oceans. When the north Atlantic flow is weak, these heating anomalies are generally reversed. Thus, the individual midlatitude jets may be influenced by more than one tropical heat source.

In addition to this relatively direct forcing from a nearby tropical heat source, the jets may be influenced by relatively remote tropical heat sources, whose signals propagate through upstream jets.

These results suggest that a clearer understanding of tropical - extratropical interactions, and which tropical locations influence which extratropical locations, are essential if improvements are to be made in extended-range forecasting. The results of this study are encouraging and indicate that area-specific extratropical circulations may have clear and identifiable relationships with the global tropical heating field. However, given the many limitations discussed previously, more research is needed in order to

develop a clearer understanding of tropical-extratropical teleconnections.

APPENDIX A - FIGURES AND TABLES

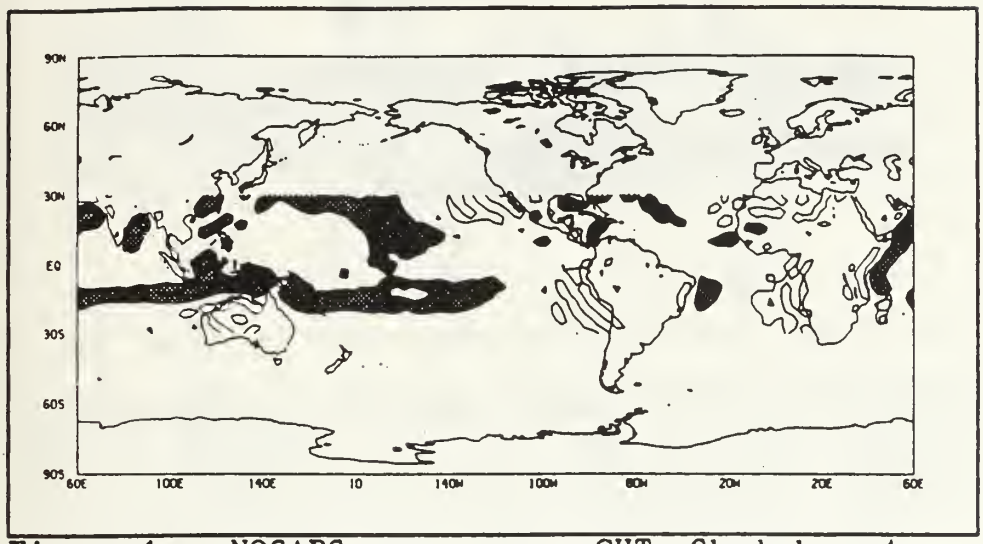

Figure 1a. NOGAPS summer mean CHT. Shaded contours represent heating greater than 1°C/day. Unshaded contours represent cooling greater than 1°C/day. Contour interval is 1°C/day.

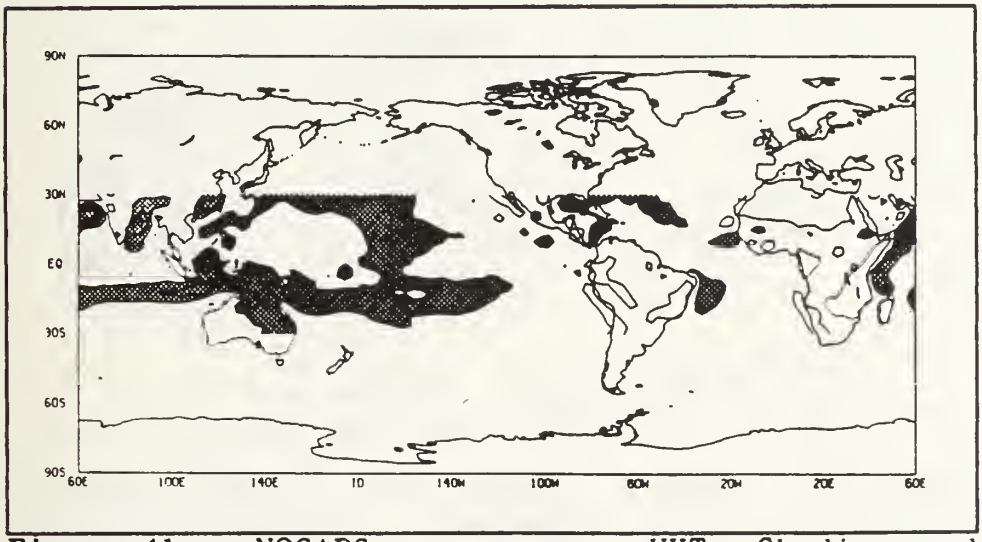

Figure 1b. NOGAPS summer mean VHT. Shading and contouring same as Figure 1a.

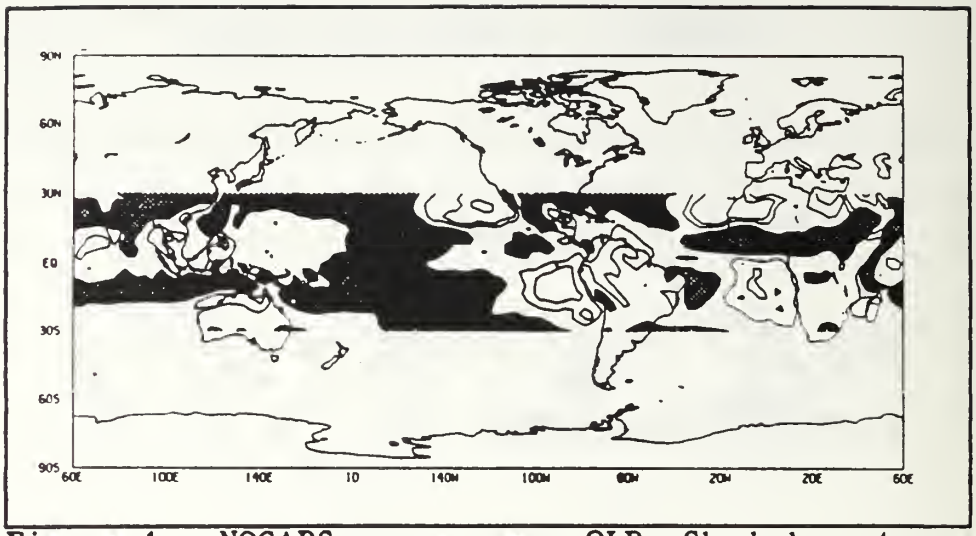

Figure 1c. NOGAPS summer mean OLR. Shaded contours indicate OLR less than 230 W m^{-2}. Unshaded contours indicate OLR greater than 270 W m^{-2}. Contour interval is 20 W m^{-2}.

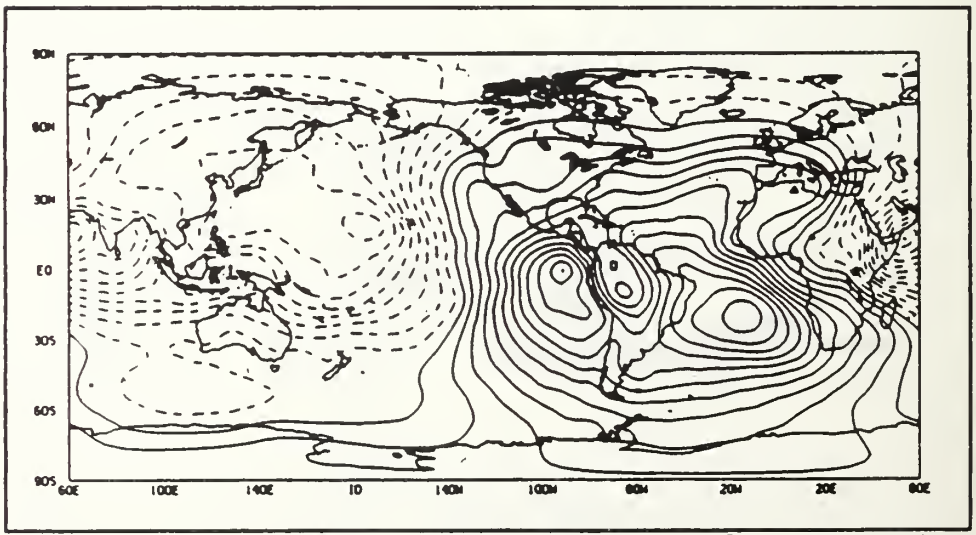

Figure 1d. NOGAPS summer mean 200mb velocity potential. Solid (dashed) contours indicate positive (negative) values. Contour interval is 10^6 m^2 s^{-1}.

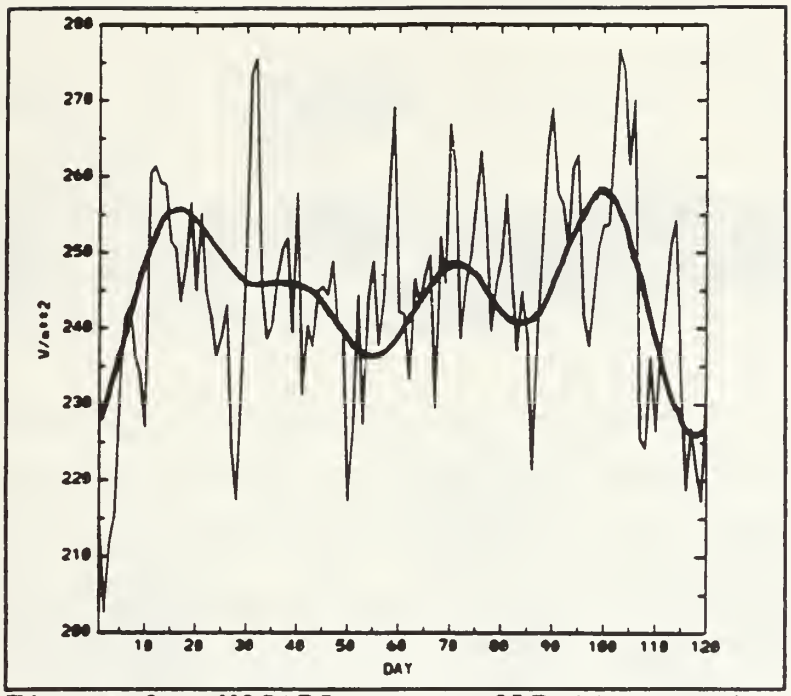

Figure 2. NOGAPS summer OLR time series for tropical western Pacific (5°N-25°N, 100°E-150°E). Heavy smooth curve represents POLR (processed) values.

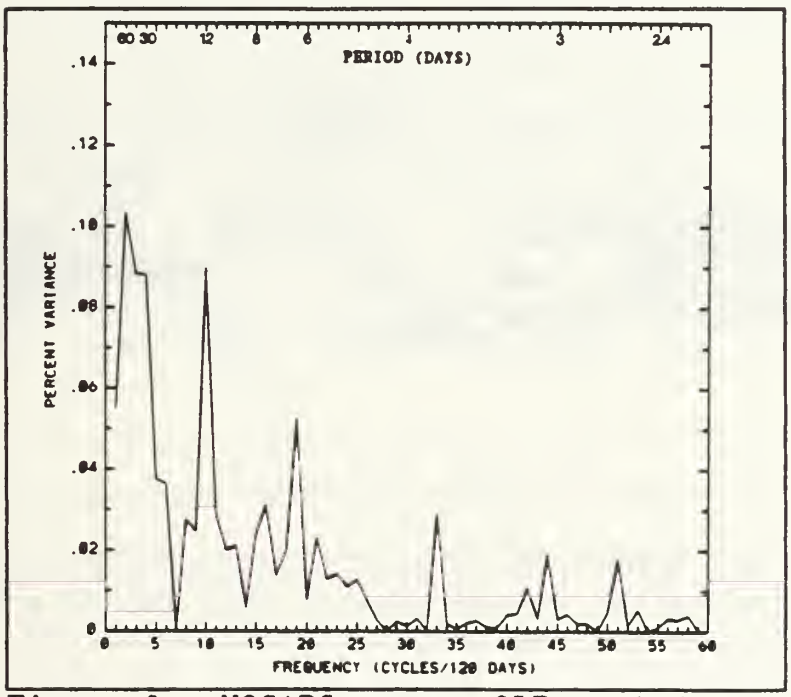

Figure 3. NOGAPS summer OLR periodogram for tropical western Pacific unprocessed time series shown in Figure 2.

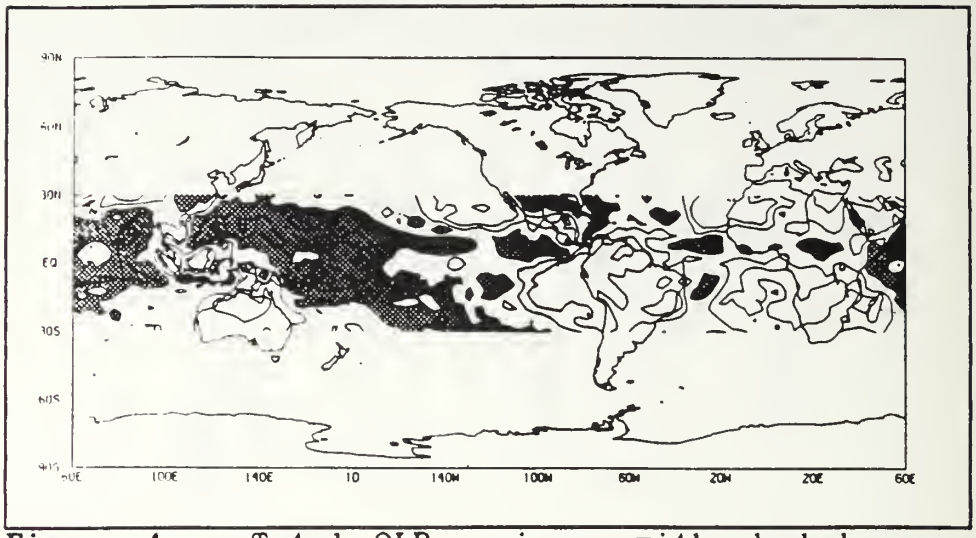

Figure 4a. Total OLR variance with shaded areas indicating values greater than 3×10^3 $(W\ m^{-2})^2$. Contour interval and lowest contour equal 10^3 $(W\ m^{-2})^2$.

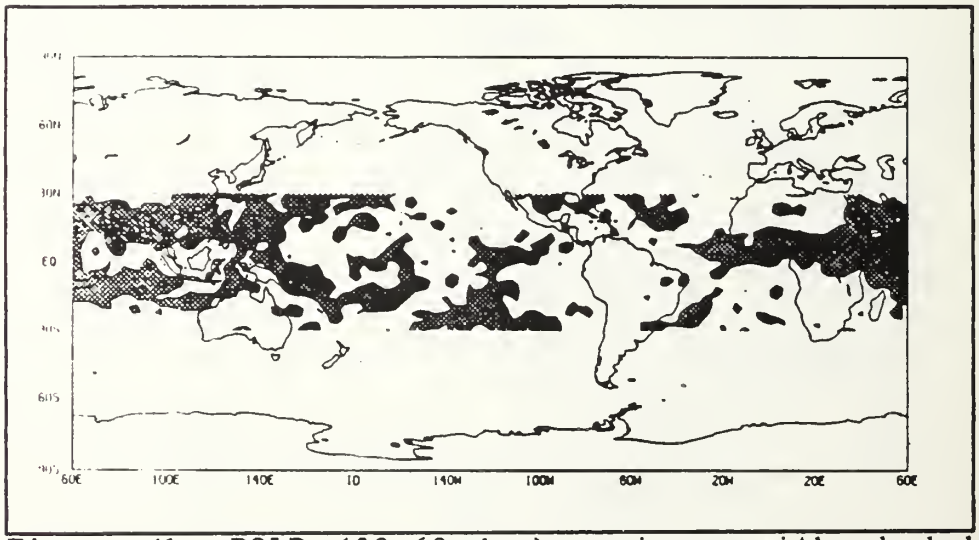

Figure 4b. POLR (30-60 day) variance with shaded areas indicating values greater than 250 $(W\ m^{-2})^2$. Contour interval and lowest contour equal 250 $(W\ m^{-2})^2$.

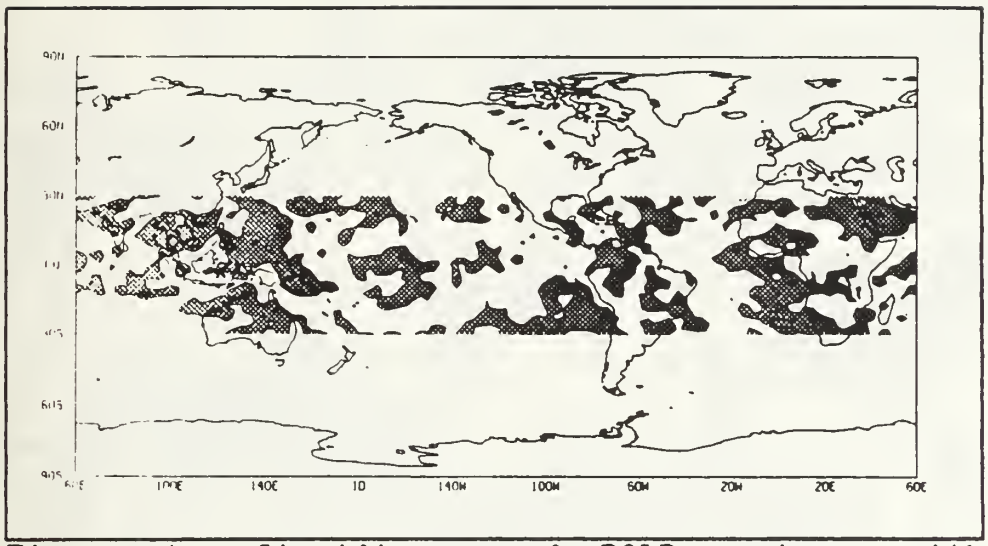

Figure 4c. Significance of POLR variance with shaded areas indicating where POLR variance exceeds a red noise background variance at the 99% significance level.

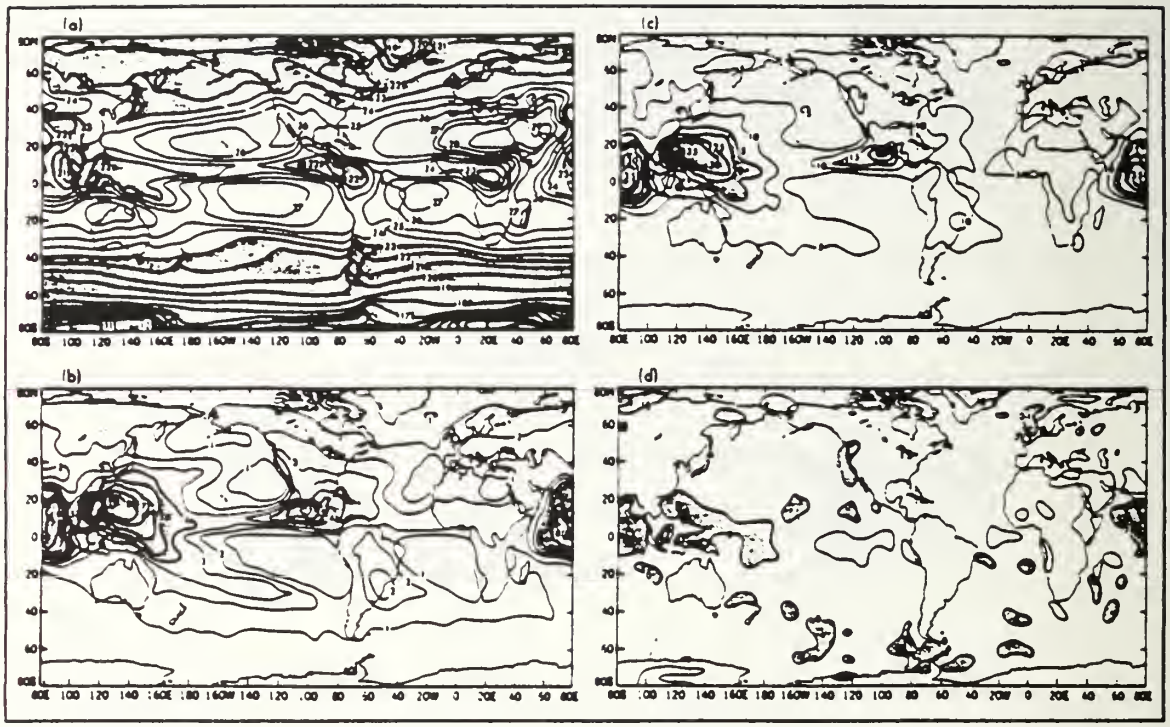

Figure 5. From Knutson et al. (1986), Figure 1. OLR statistics based on nine NH summers: a) Mean OLR with shading indicating values less than 230 W m^{-2}. b) Total OLR variance with shaded areas indicating values greater than 400 $(W\ m^{-2})^2$. Contour interval is 100 $(W\ m^{-2})^2$. Labels are divided by 100. c) 28-72 day variance with shaded areas indicating values greater than 150 $(W\ m^{-2})^2$. Contour interval is 50 $(W\ m^{-2})^2$. Labels are divided by 10. d) Shaded regions indicate where 28-72 day OLR variance exceeds a red noise background variance at the 95% significance level.

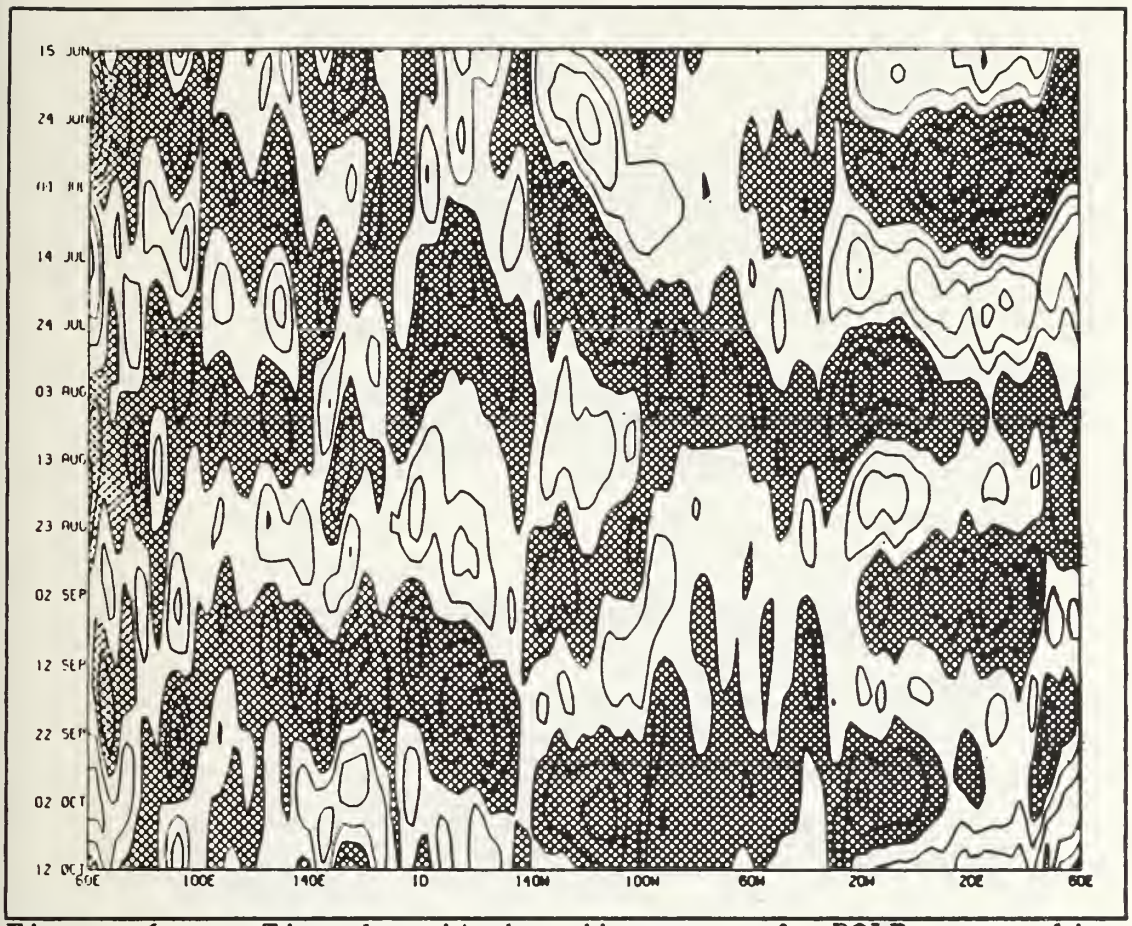

Figure 6. Time-longitude diagram of POLR anomalies averaged over 5°S-5°N, for NOGAPS summer. Contour interval is 10 W m^{-2}. Shading indicates negative POLR (positive heating) anomalies.

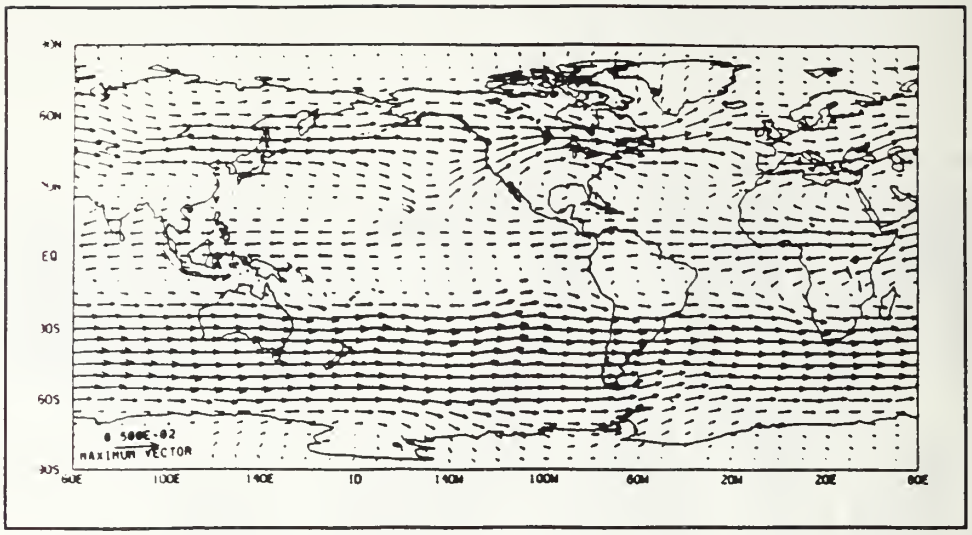

Figure 7a. NOGAPS summer mean 200mb vector wind field.

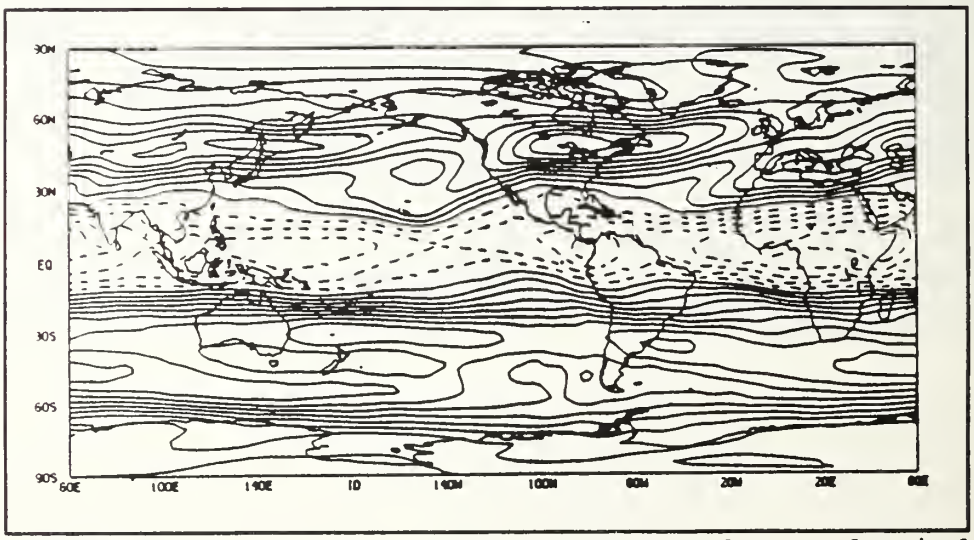

Figure 7b. NOGAPS summer mean 200mb zonal wind (U200) field. Contour interval is 5 m s^{-1}. Solid (dashed) contours indicate positive (negative) U200 velocities.

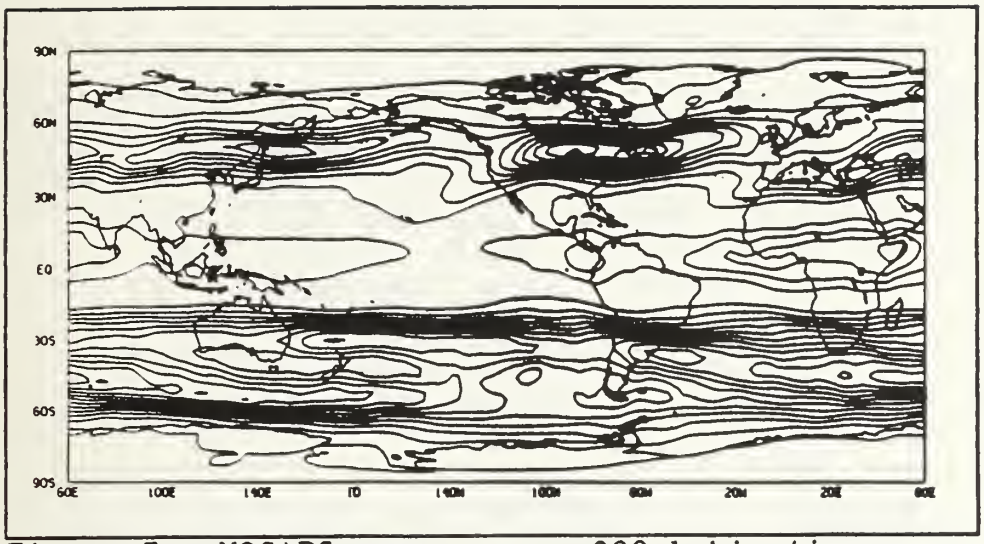

Figure 7c. NOGAPS summer mean 200mb kinetic energy field. Contour interval is 100 $(m\ s^{-1})^2$.

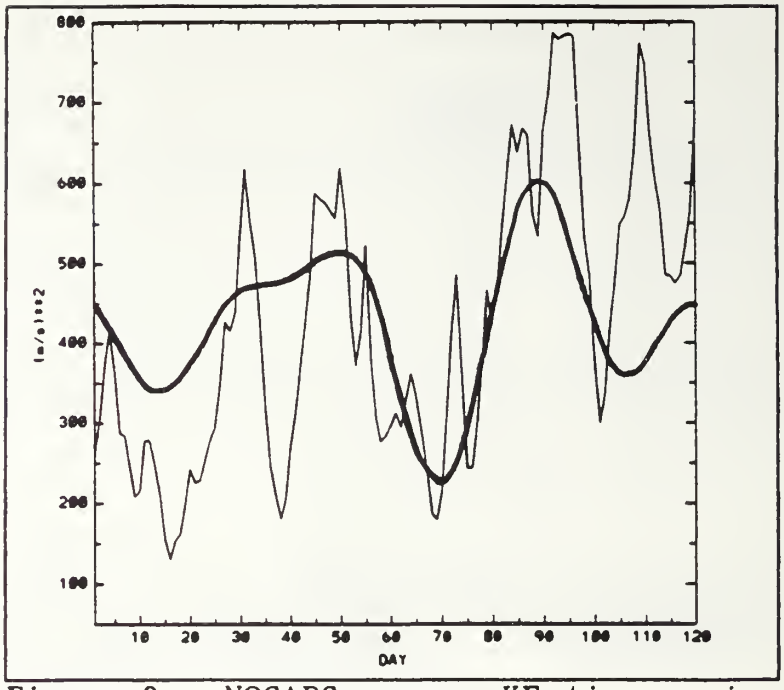

Figure 8. NOGAPS summer KE time series for extratropical North Pacific (NP). Heavy, smooth curve represents PKE (processed) values.

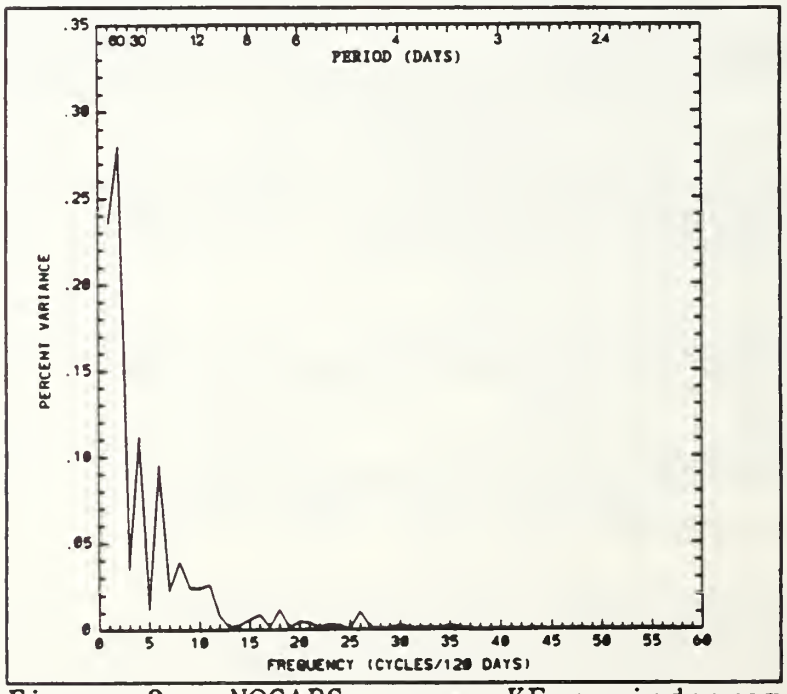

Figure 9. NOGAPS summer KE periodogram for extratropical NP unprocessed time series shown in Figure 8.

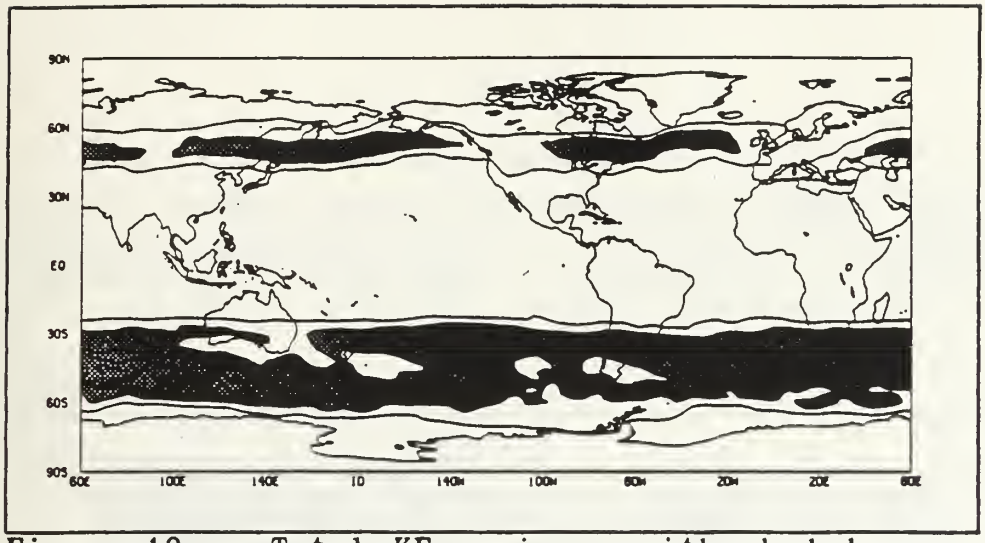

Figure 10a. Total KE variance with shaded areas indicating values greater than 10^5 $(m^2\ s^{-2})^2$. Contour interval is $5x10^4$ $(m^2\ s^{-2})^2$. Lowest contour is 0.0.

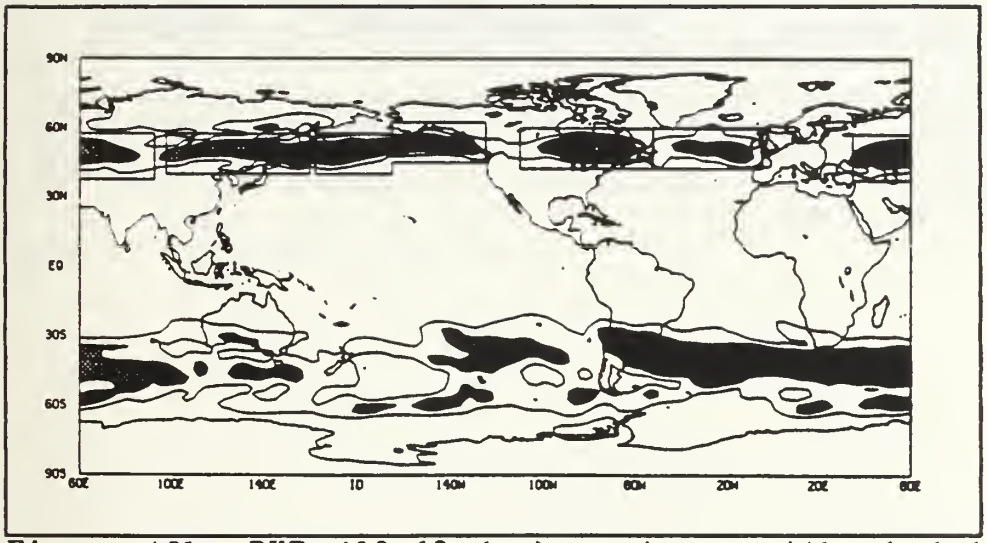

Figure 10b. PKE (30-60 day) variance with shaded areas indicating values greater than $4x10^4$ $(m^2 s^{-2})^2$. Contour interval is $2x10^4$ $(m^2\ s^{-2})^2$. Lowest contour is 0.0.

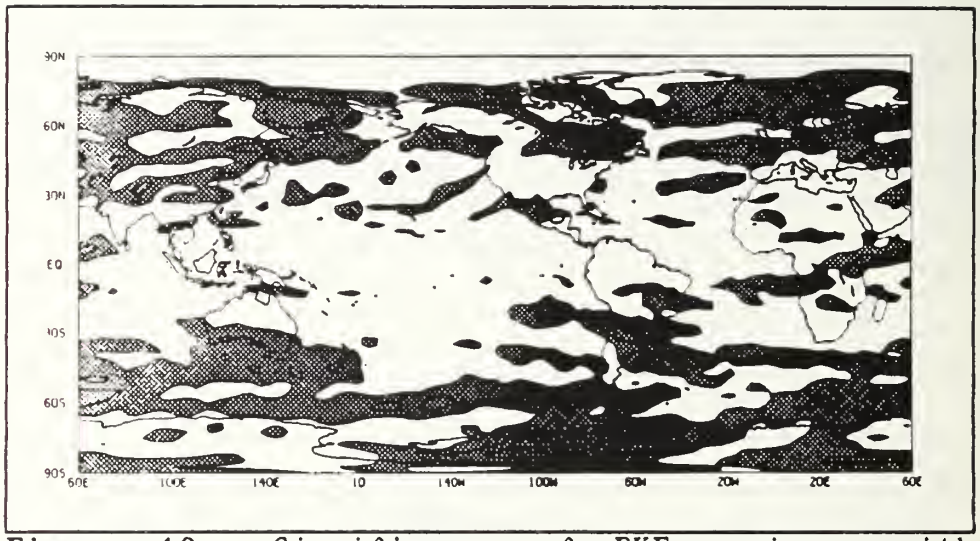

Figure 10c. Significance of PKE variance with shaded areas indicating where PKE variance exceeds a red noise background variance at the 99% significance level.

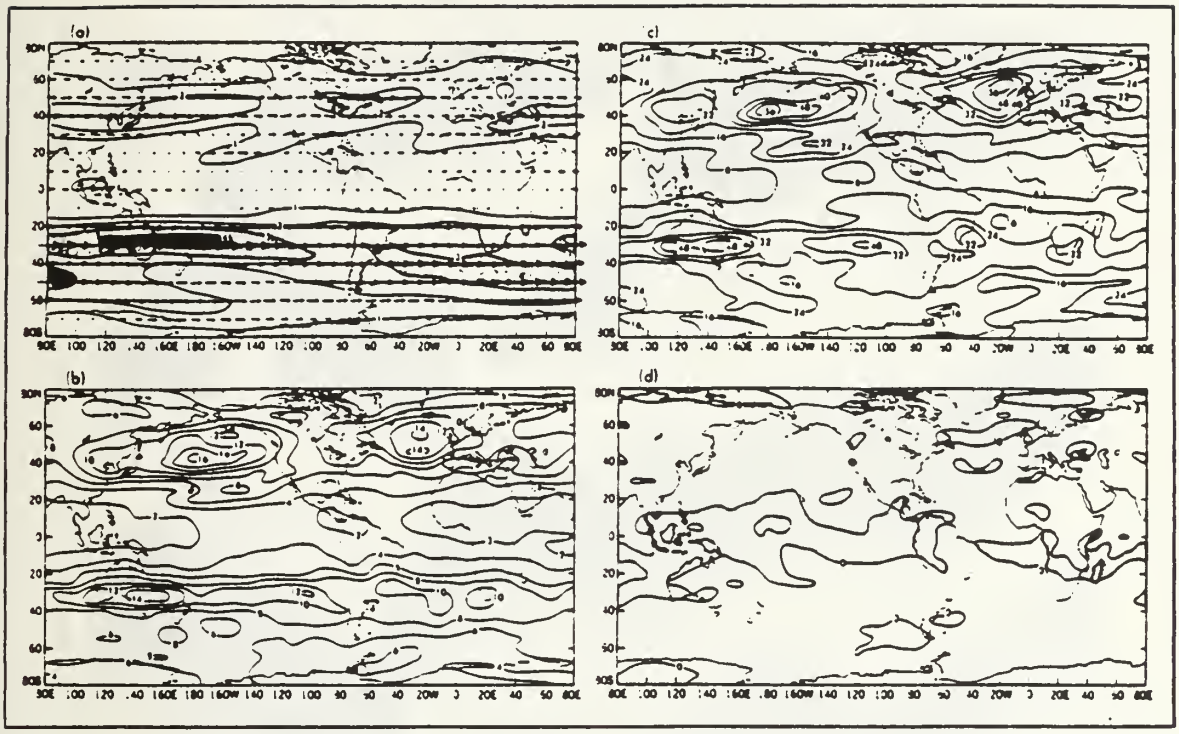

Figure 11. From Knutson et al. (1986), Figure 2. 250mb wind field statistics based on nine NH summers: a) Mean vector wind field. Contour labels are divided by 10. b) Total variance of 250mb zonal wind (U250). Contour labels are divided by 10. c) U250 28-72 day variance. d) Shaded regions indicate where 28-72 day U250 variance exceeds a red noise background variance at the 95% significance level.

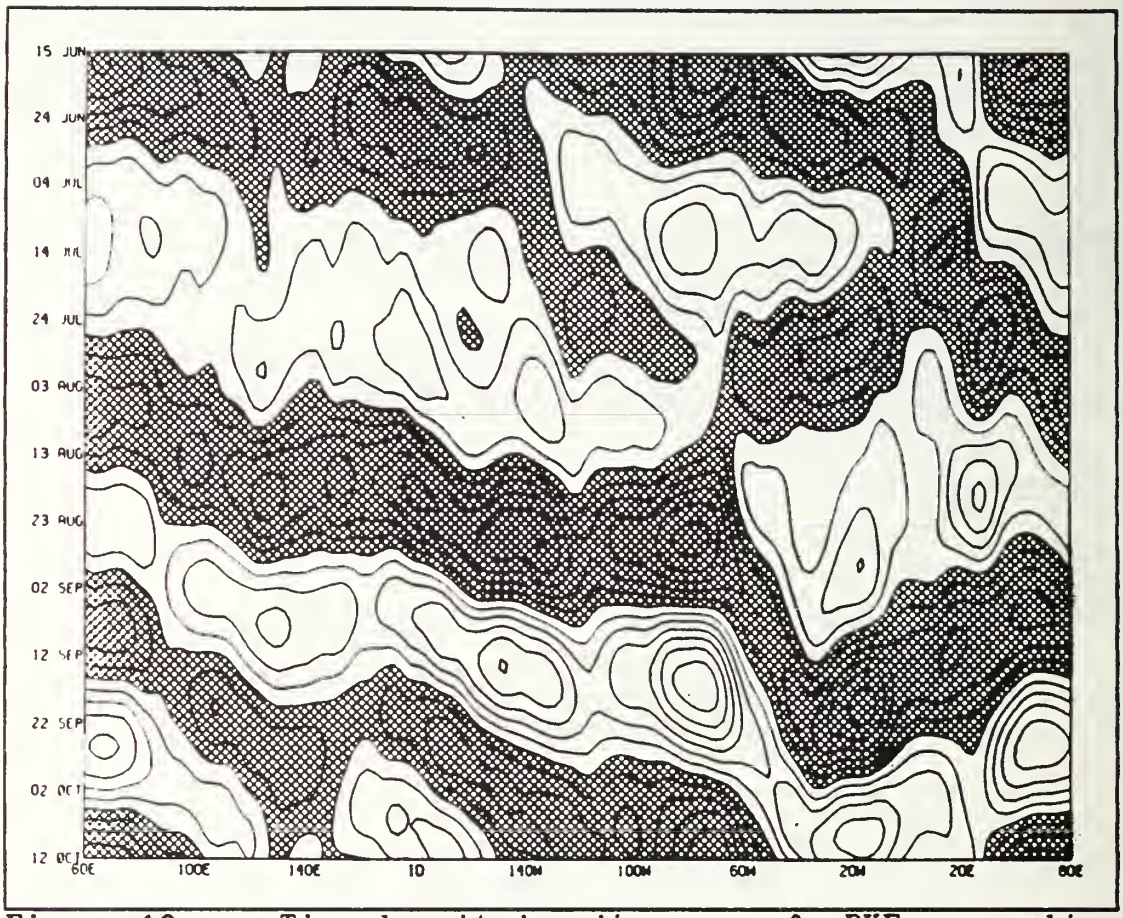

Figure 12. Time-longitude diagram of PKE anomalies averaged over 40°N-60°N, for NOGAPS summer. Contour interval is 50 m^2 s^{-2}. Shading indicates negative PKE (reduced jet strength) anomalies.

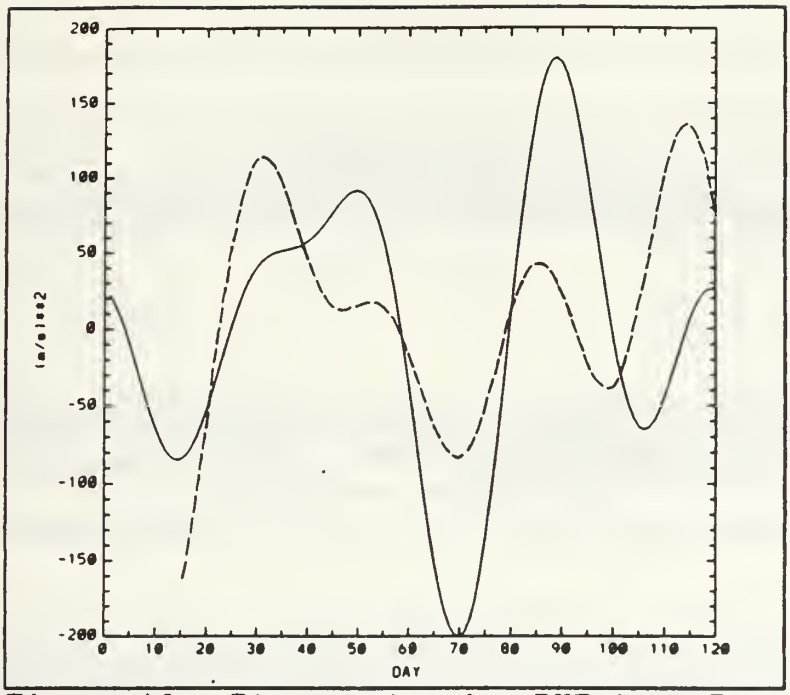

Figure 13. Time series for PKE from Fig. 8 (solid) and POLR from Fig. 2 (dashed). POLR shifted forward by 14 days (i.e., POLR day = PKE day - 14).

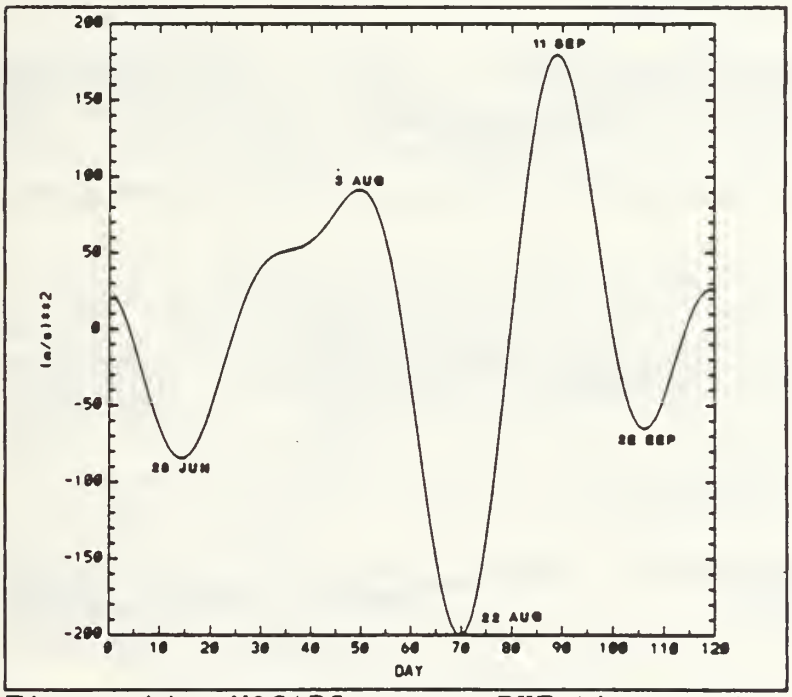

Figure 14. NOGAPS summer PKE time series for extratropical North Pacific (NP) with dates of relative maximum (minimum) PKE anomalies indicated.

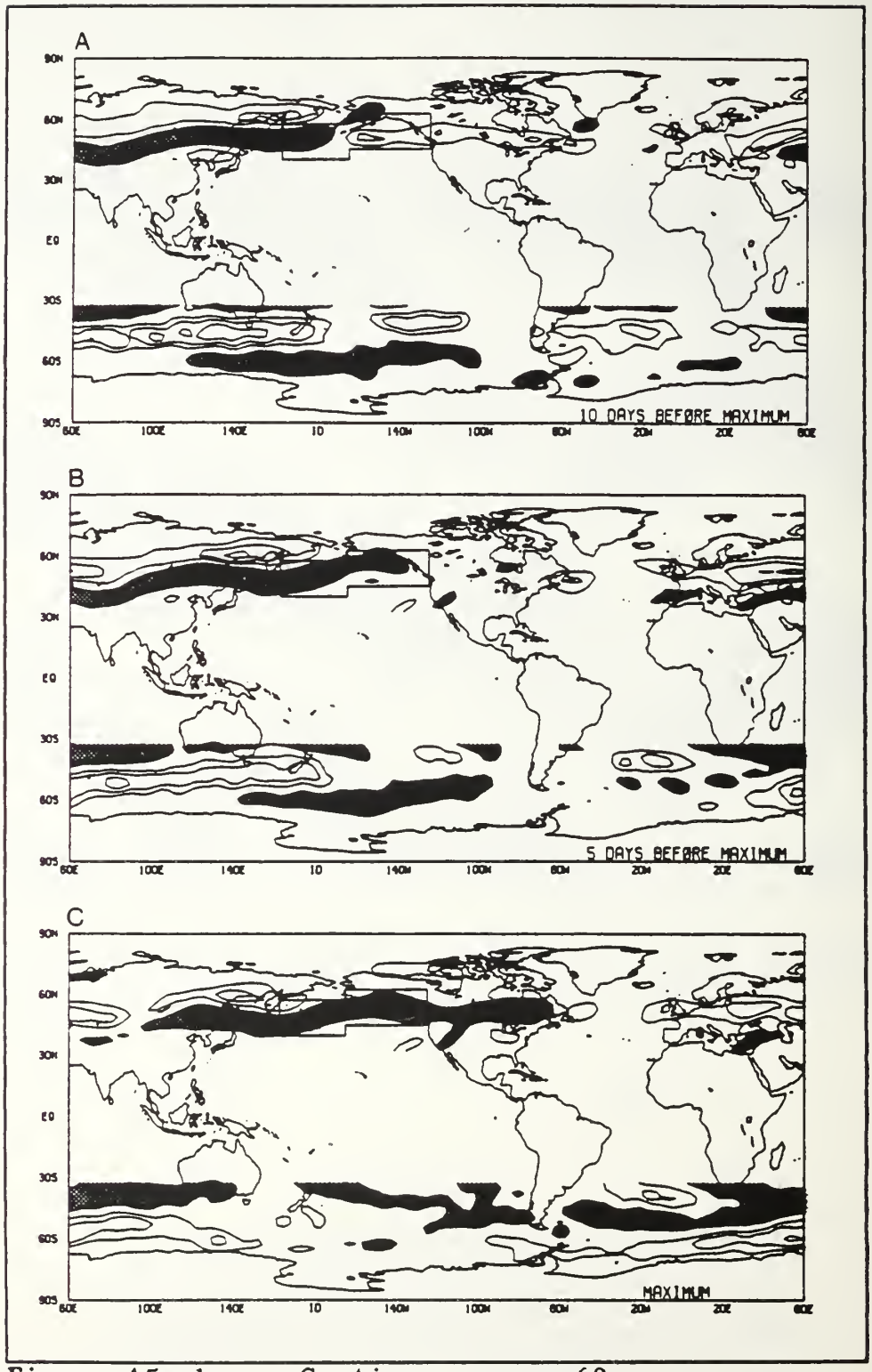

Figure 15a,b,c. Caption on page 69.

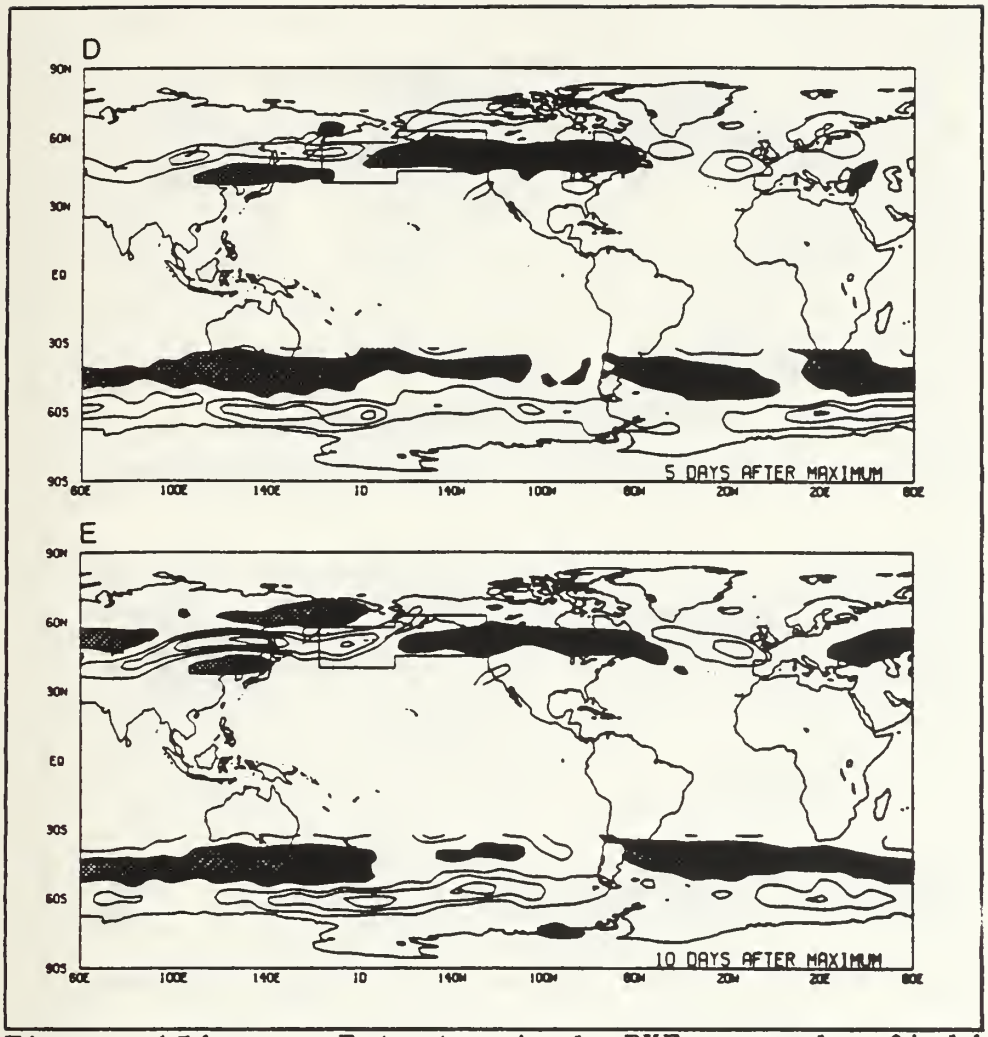

Figure 15d,e. Extratropical PKE anomaly field before, during and after the composite PKE anomaly maximum in the North Pacific (NP) boxed region: (a) 10 days before maximum. (b) 5 days before maximum. (c) at maximum. (d) 5 days after maximum. (e) 10 days after maximum. Contour interval is 100 (m s^{-1})^2 with lowest contoured value equal to ±100 (m s^{-1})^2. Shaded (unshaded) contours indicate positive (negative) PKE anomalies which represent enhanced (reduced) jet strength.

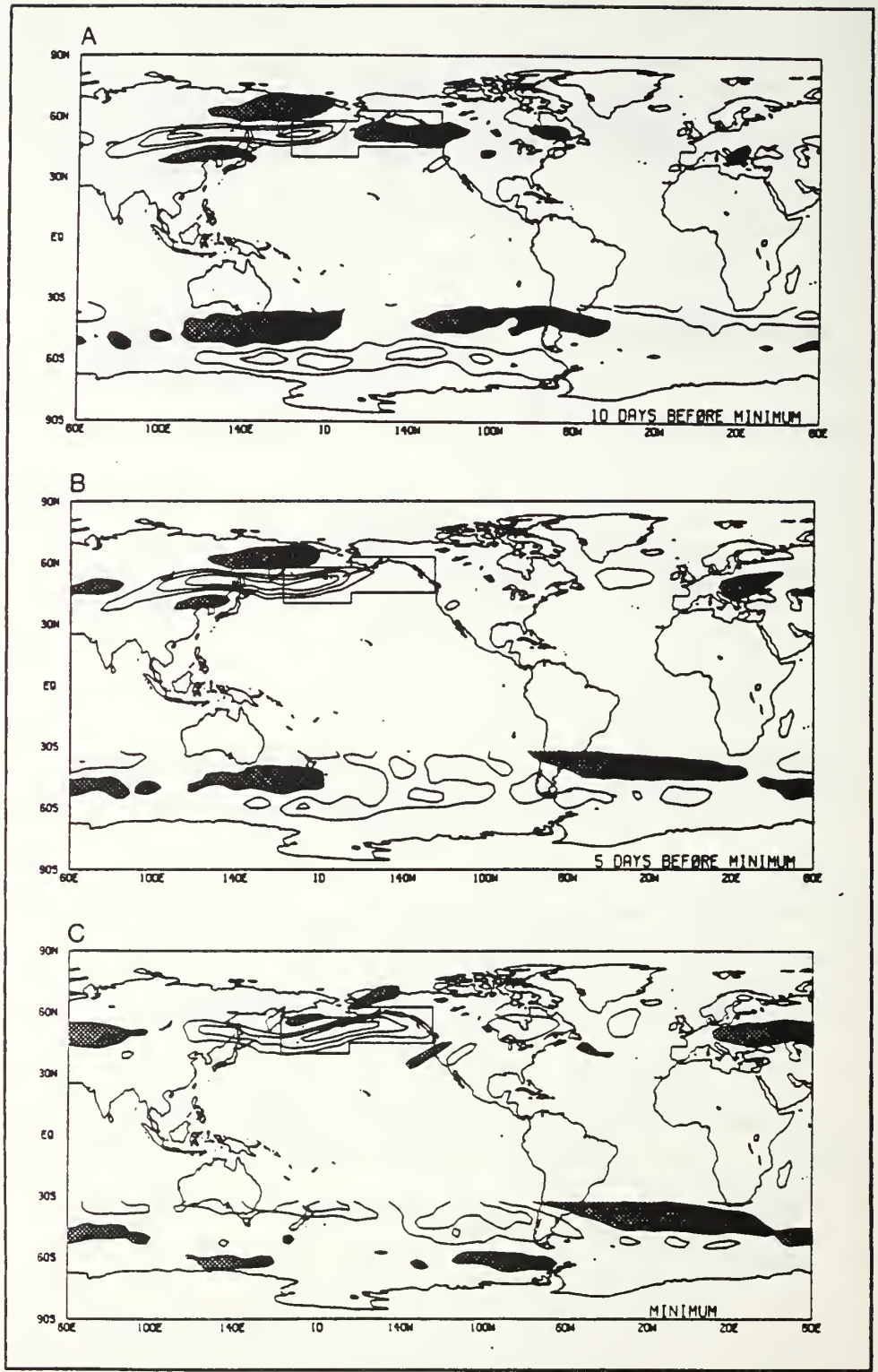

Figure 16a,b,c. Caption on page 71.

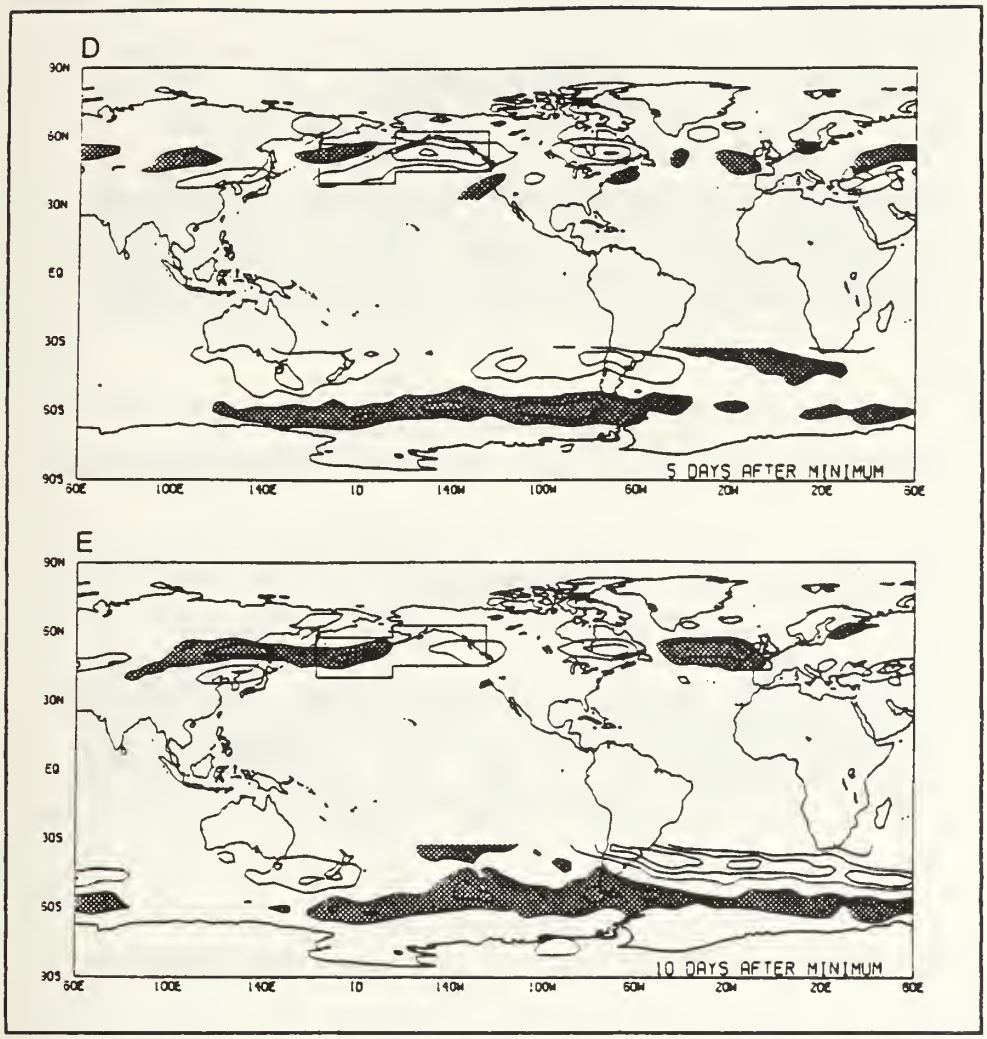

Figure 16d,e. Extratropical PKE anomaly field before, during, and after the composite PKE anomaly minimum in the North Pacific (NP) boxed region: (a) 10 days before minimum. (b) 5 days before minimum. (c) at minimum. (d) 5 days after minimum. (e) 10 days after minimum. Contour interval is 100 (m s^{-1})^2 with lowest contoured value equal to ±100 (m s^{-1})^2. Shaded (unshaded) contours indicate positive (negative) PKE anomalies which represent enhanced (reduced) jet strength.

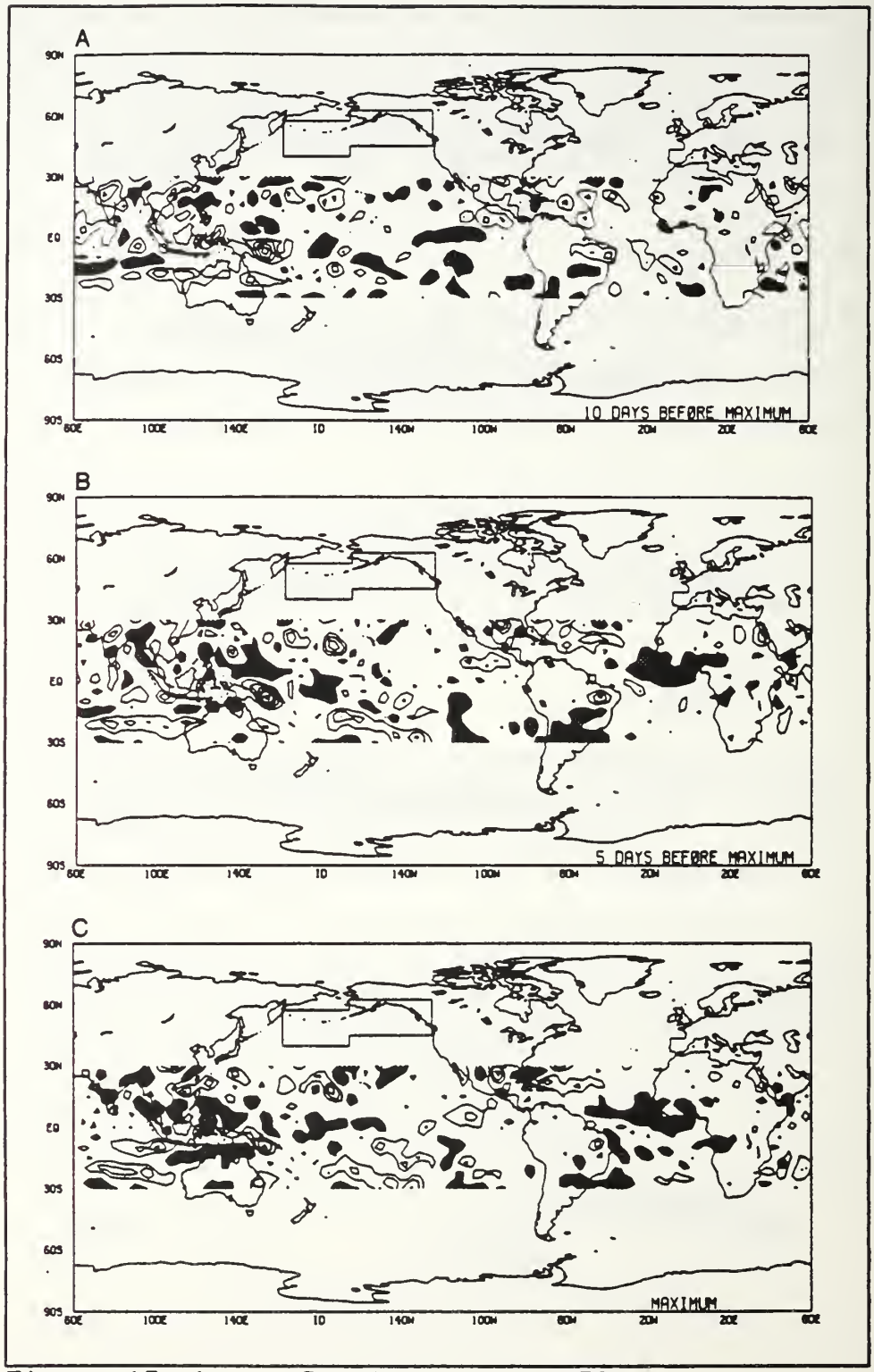

Figure 17a,b,c. Caption on page 73.

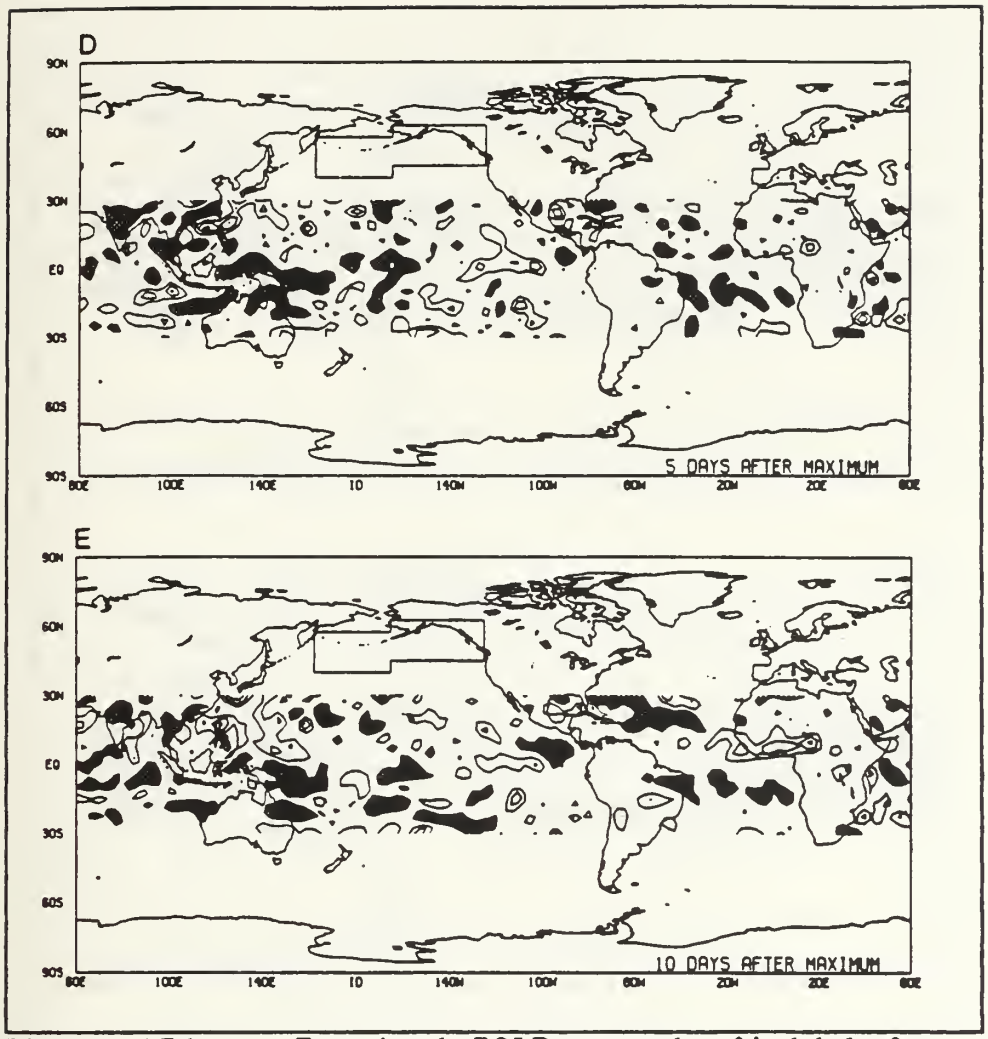

Figure 17d,e. Tropical POLR anomaly field before, during and after the composite PKE anomaly maximum in the North Pacific (NP) boxed region: (a) 10 days before maximum. (b) 5 days before maximum. (c) at maximum. (d) 5 days after maximum. (e) 10 days after maximum. Contour interval is 10 $(W\ m^{-2})^2$ with lowest contoured values equal to $\pm 10\ (W\ m^{-2})^2$. Shaded (unshaded) contours indicate negative (positive) POLR anomalies which represent enhanced (reduced) heating.

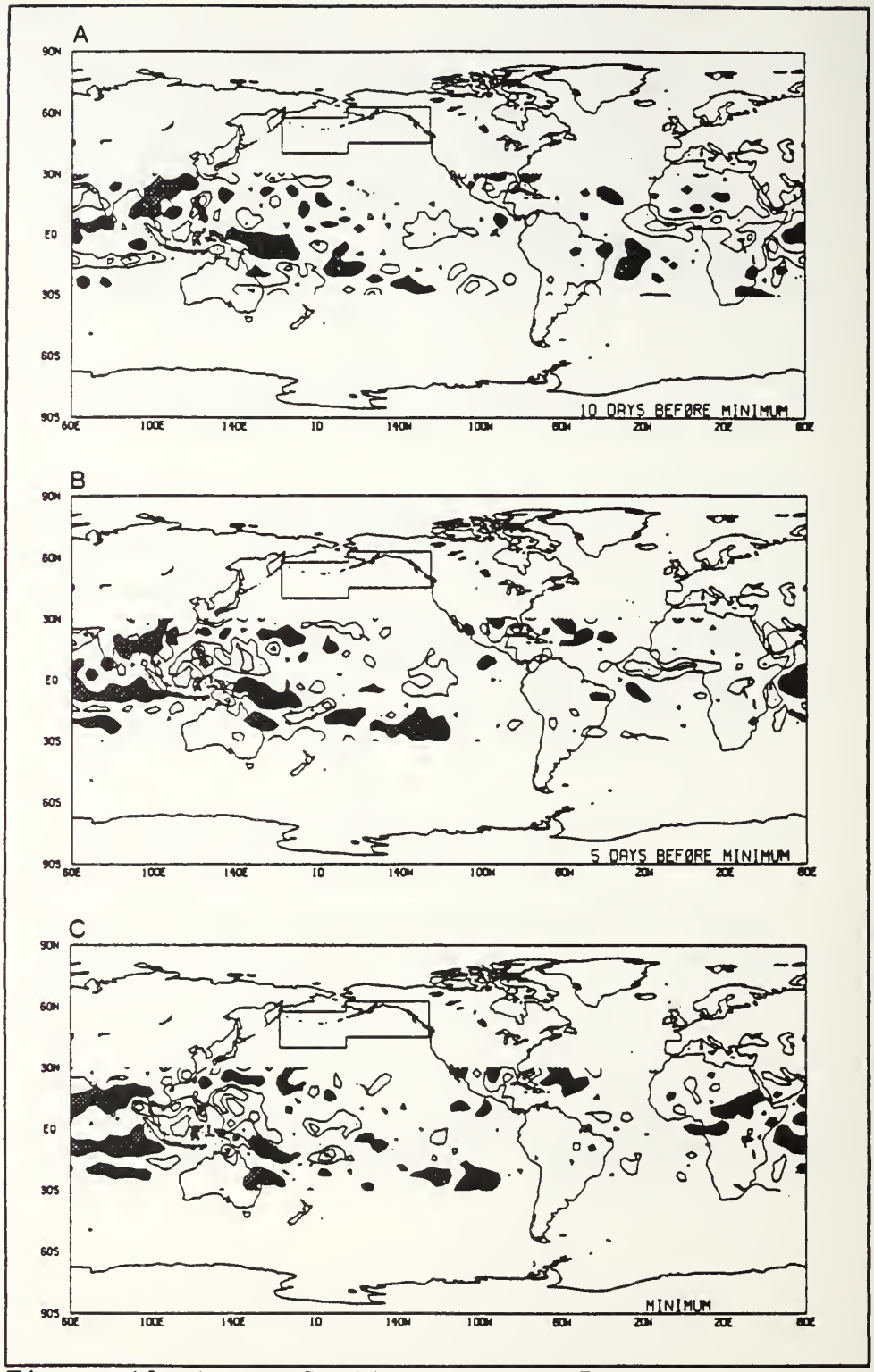

Figure 18a,b,c. Caption on page 75.

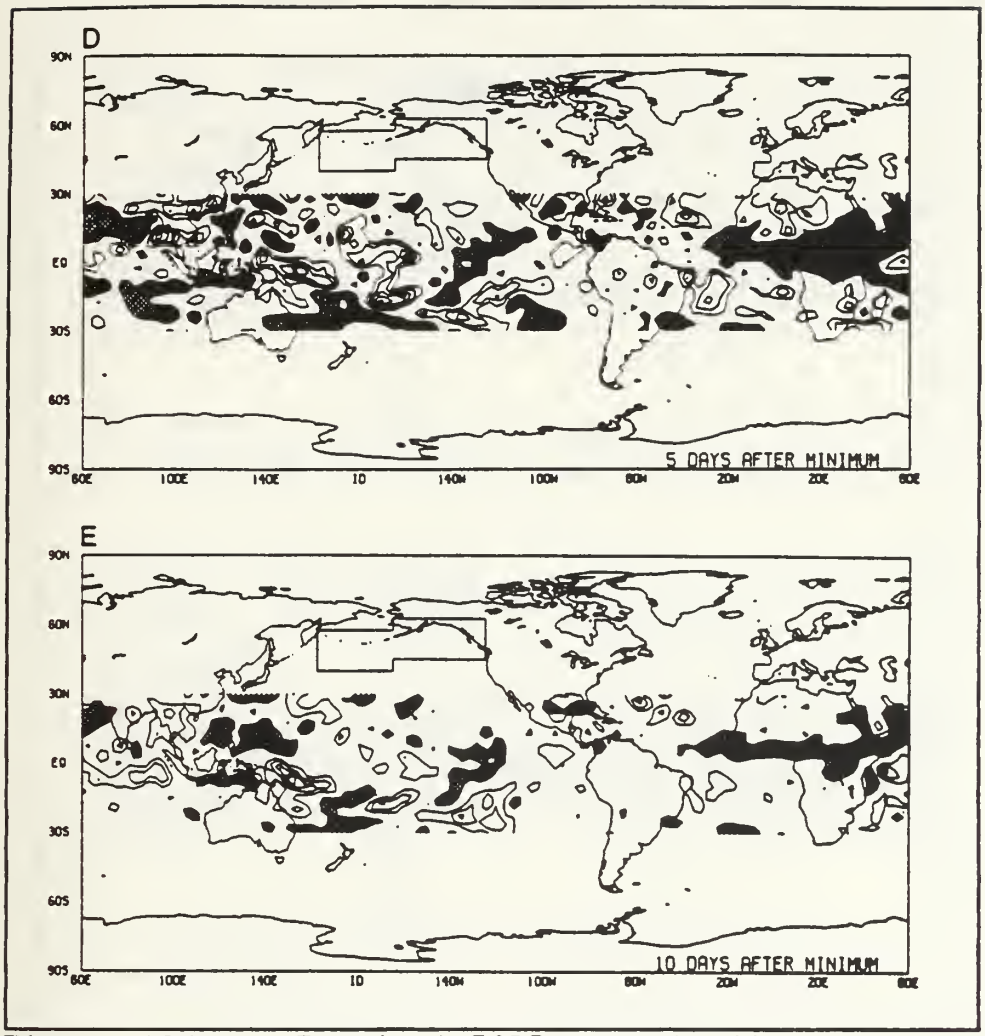

Figure 18d,e. Tropical POLR anomaly field before, during, and after the composite PKE anomaly minimum in the North Pacific (NP) boxed region: (a) 10 days before minimum. (b) 5 days before minimum. (c) at minimum. (d) 5 days after minimum. (e) 10 days after minimum. Contour interval is 10 $(W\ m^{-2})^2$ with lowest contoured values equal to $\pm 10\ (W\ m^{-2})^2$. Shaded (unshaded) contours indicate negative (positive) POLR anomalies which represent enhanced (reduced) heating.

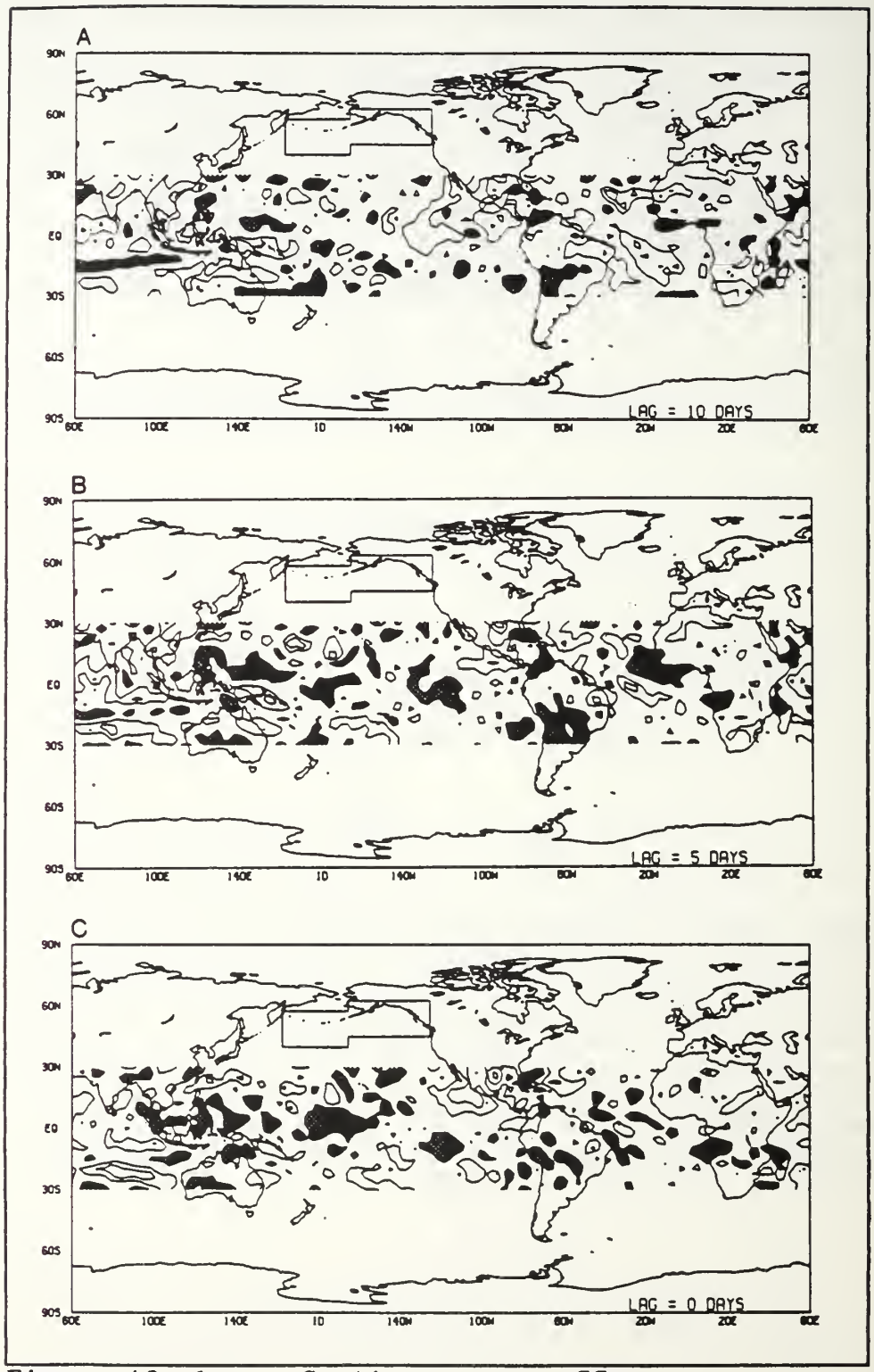

Figure 19a,b,c. Caption on page 77.

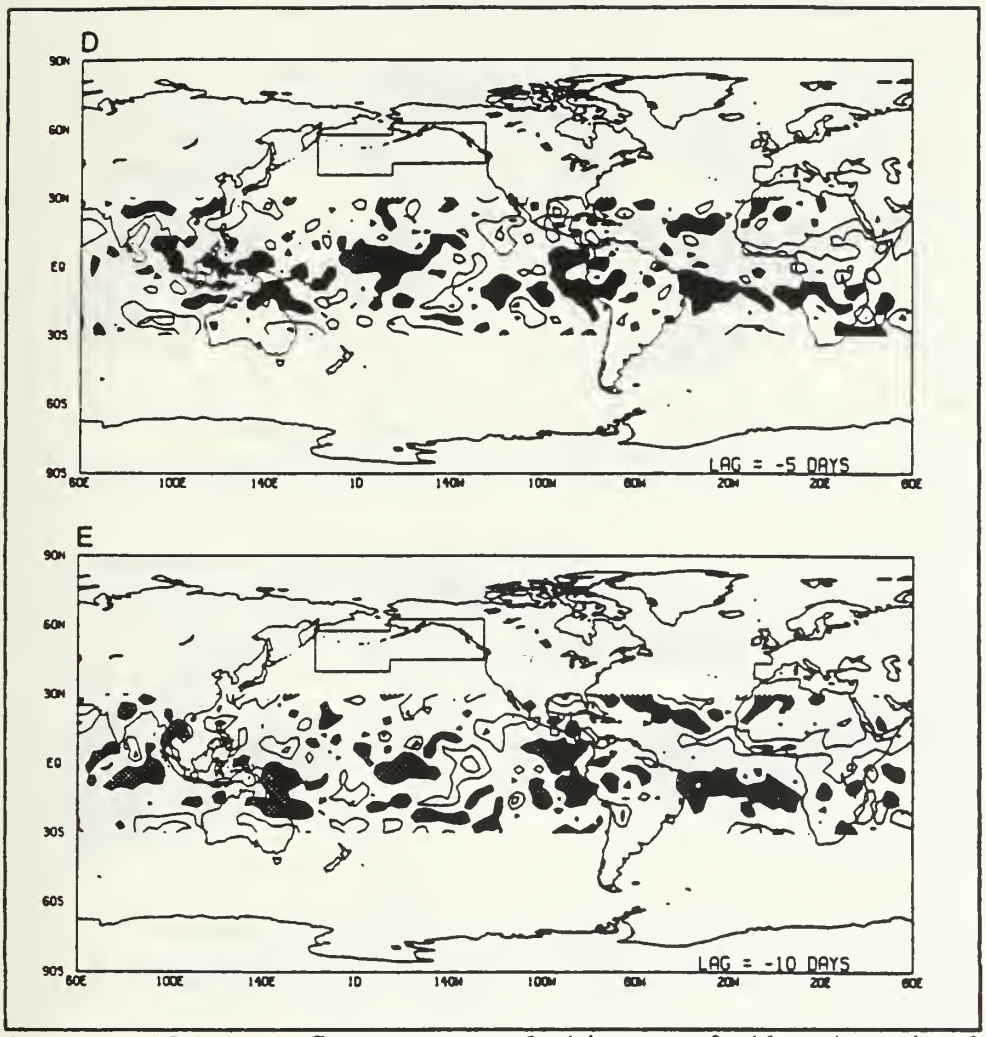

Figure 19d,e. Cross-correlations of the tropical POLR anomaly field with the North Pacific (NP) PKE anomaly time series shown in Figure 13: (a) lag = +10 days. (b) lag = +5 days. (c) lag = 0 days. (d) lag = -5 days. (e) lag = 10 days. Contour interval is 0.4 with lowest contoured value equal to ±0.4. Shaded (unshaded) contours indicate negative (positive) correlations.

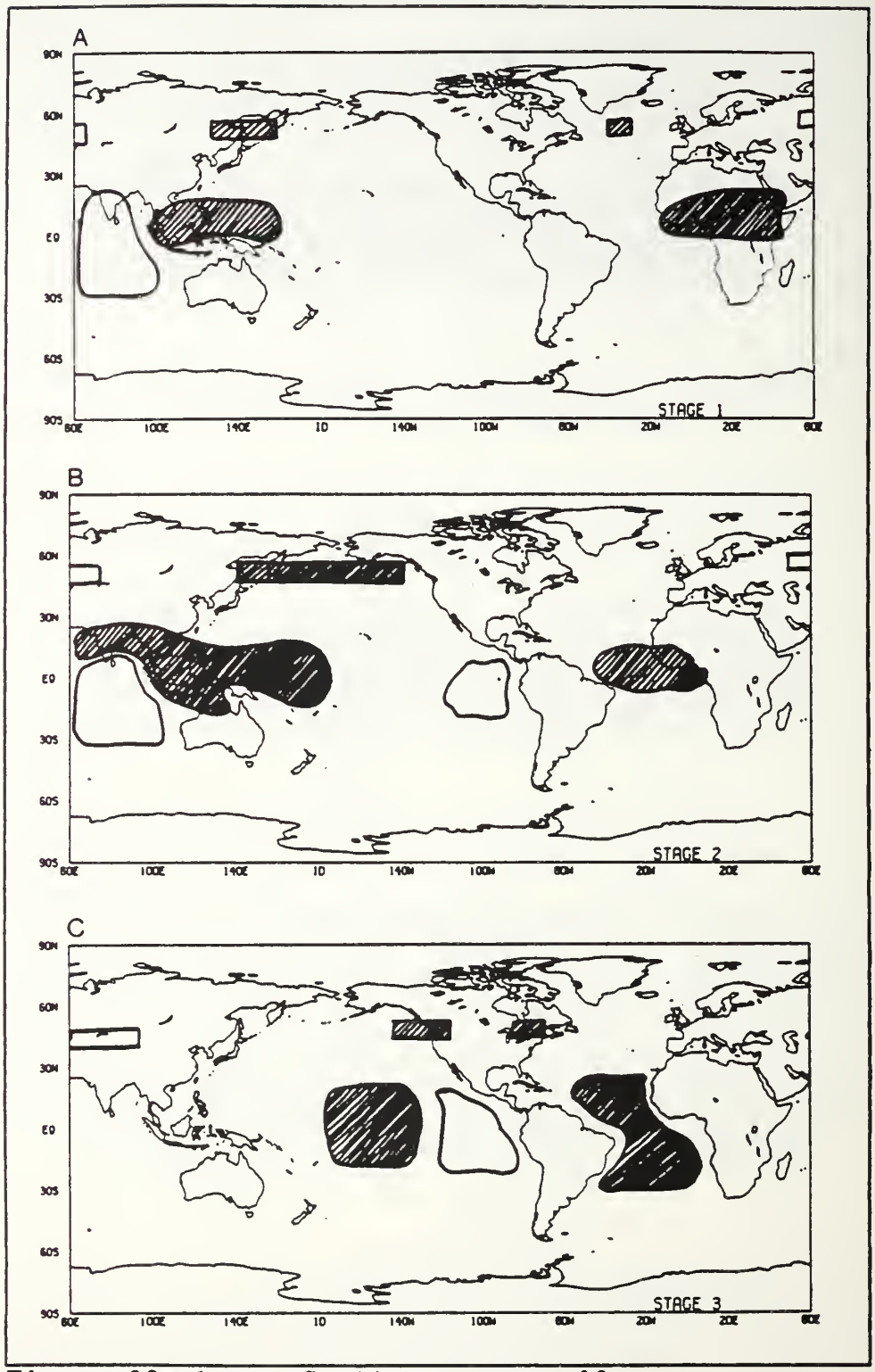

Figure 20a,b,c. Caption on page 80.

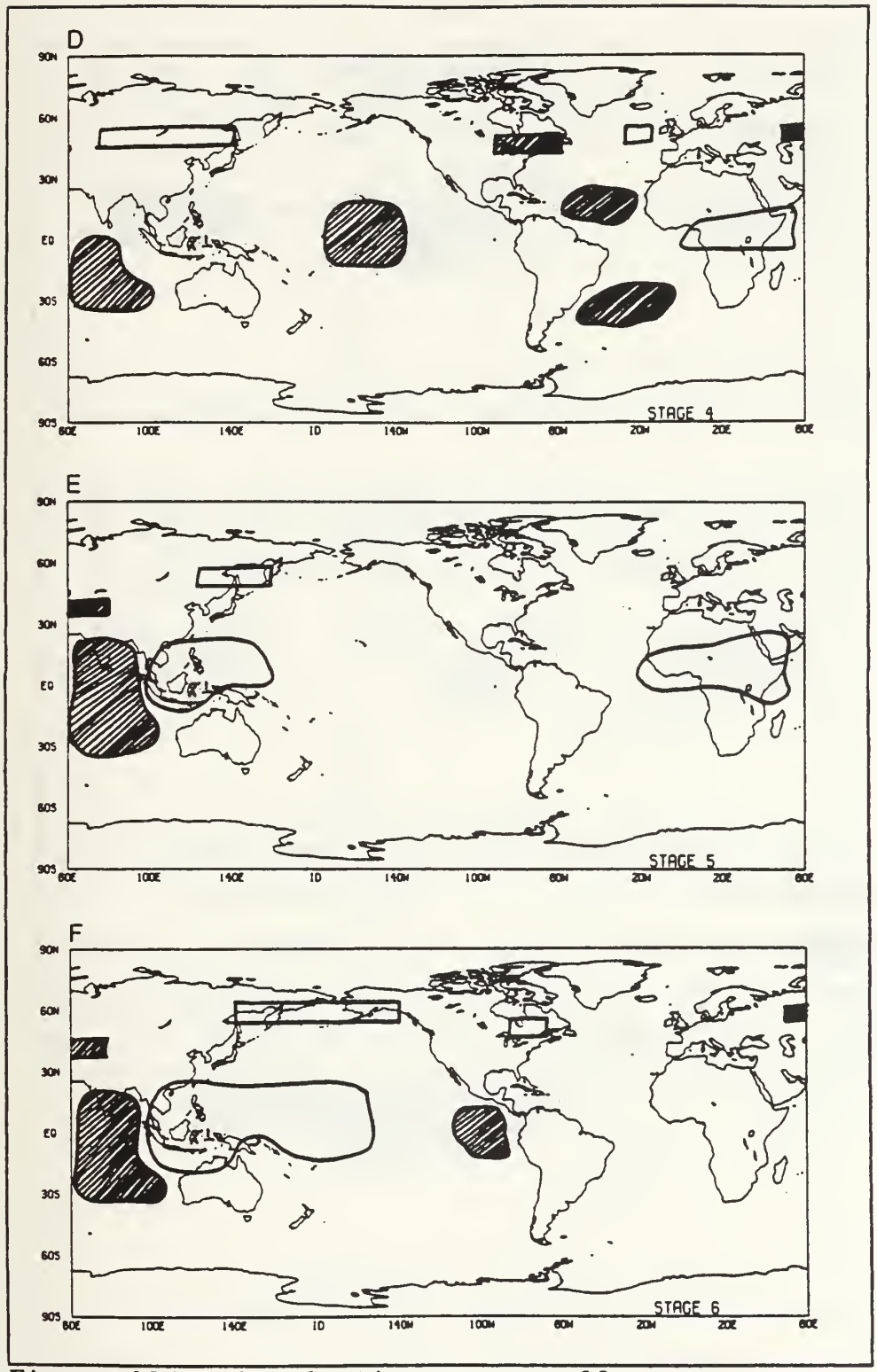

Figure 20d,e,f. Caption on page 80.

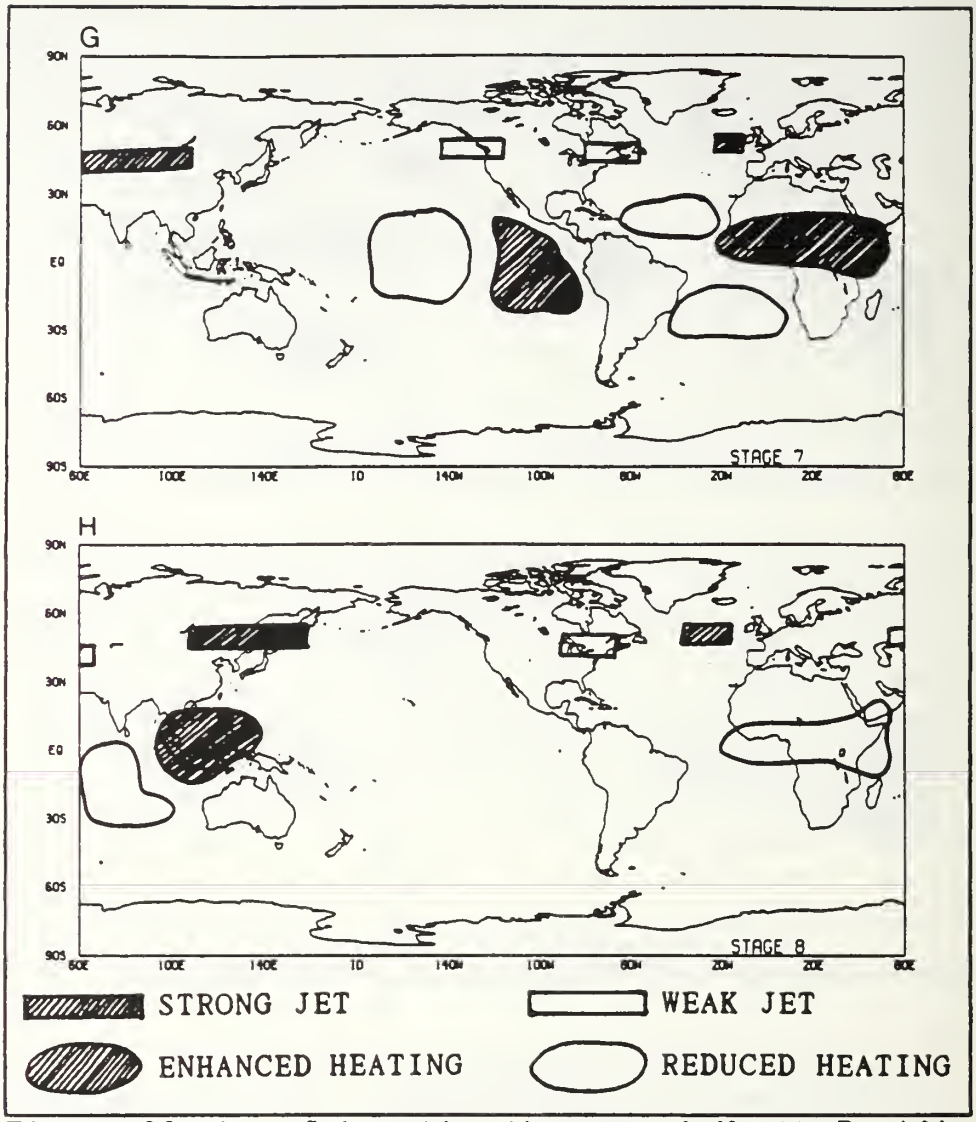

Figure 20g,h. Schematic diagram of North Pacific jet life-cycle and relationship to global tropical heating. Panels a - h represent Stages 1 through 8, as discussed in Chapter III, Section C.1.d.

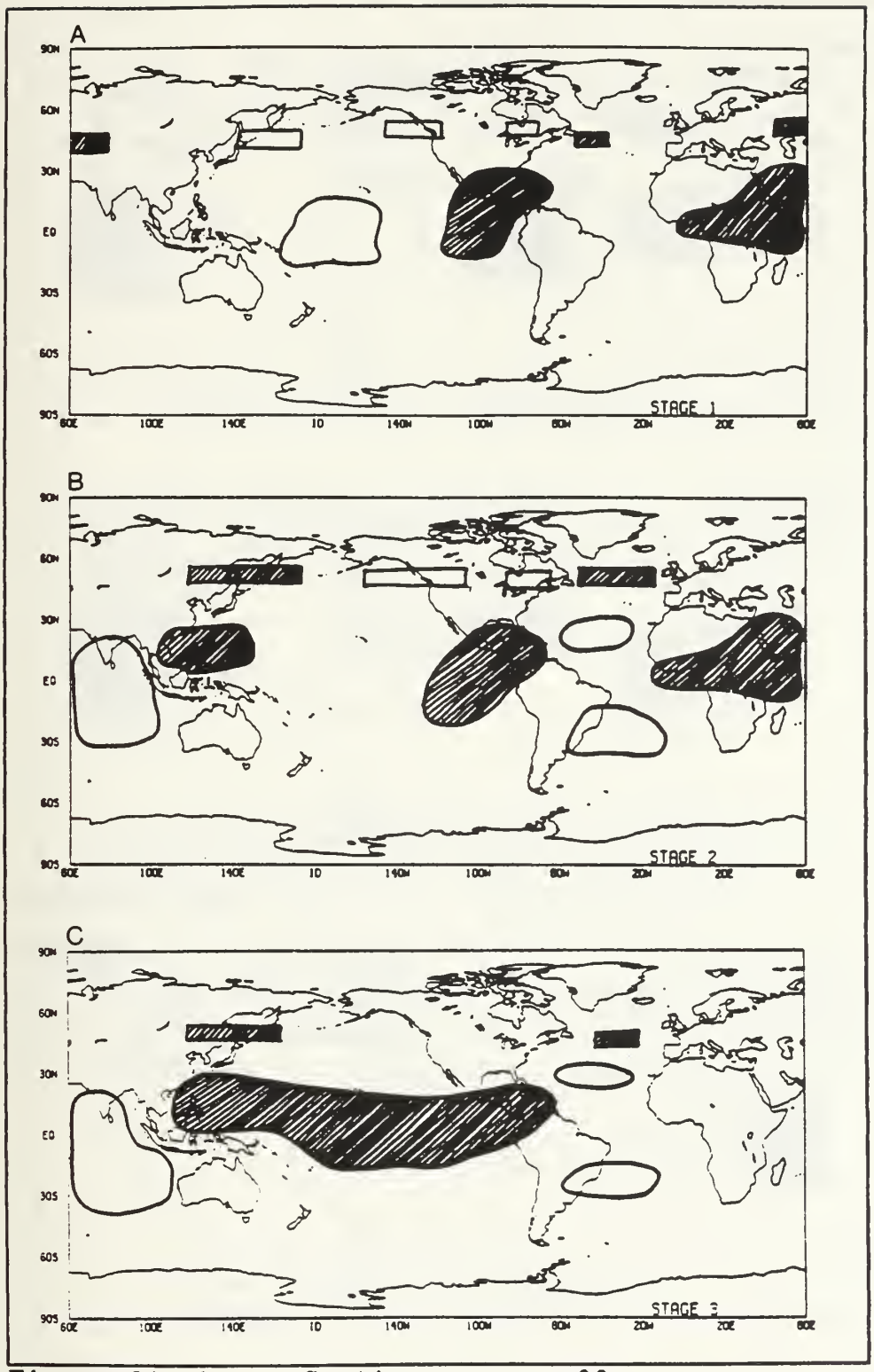

Figure 21a,b,c. Caption on page 83.

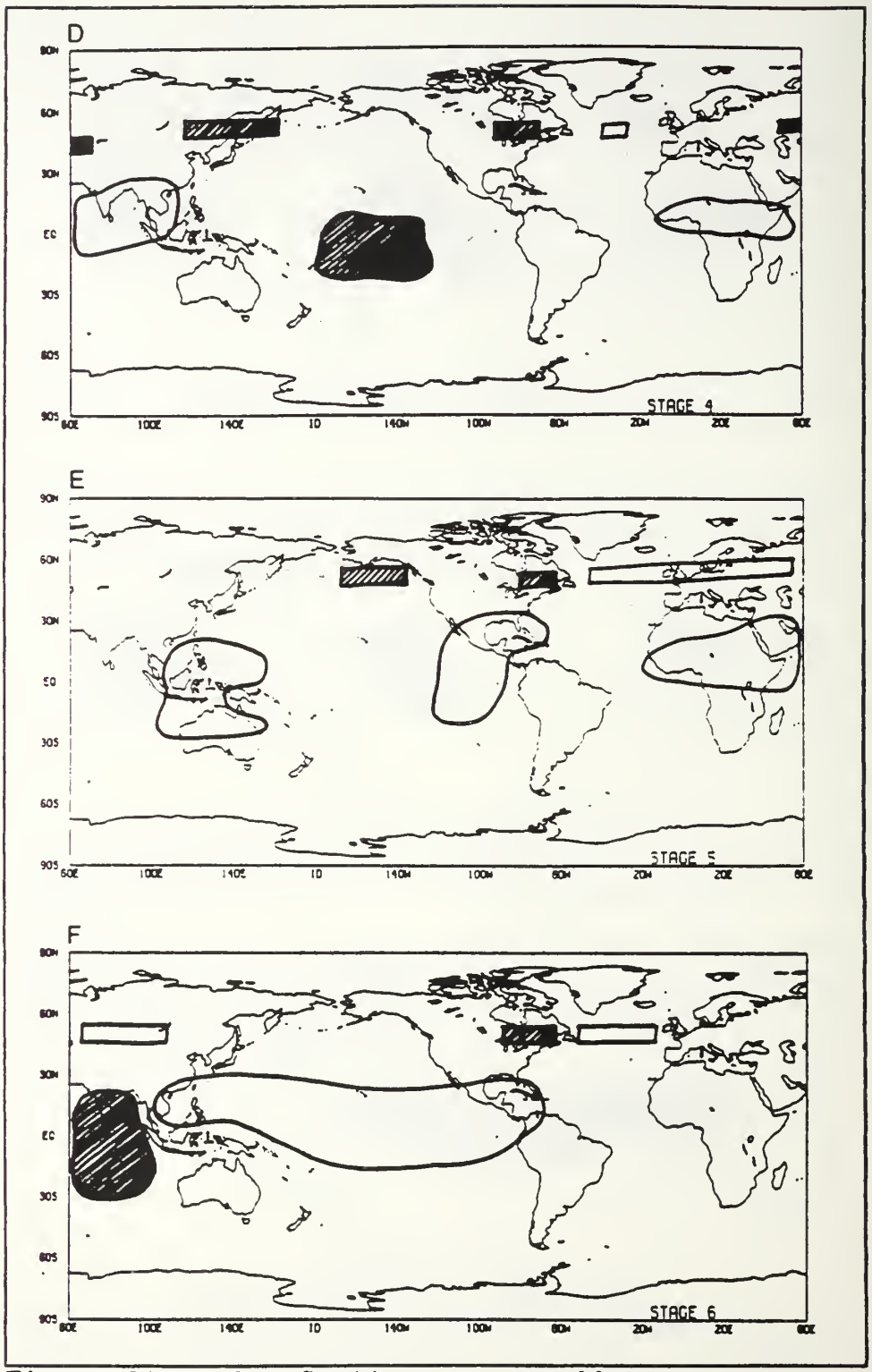

Figure 21d,e,f. Caption on page 83.

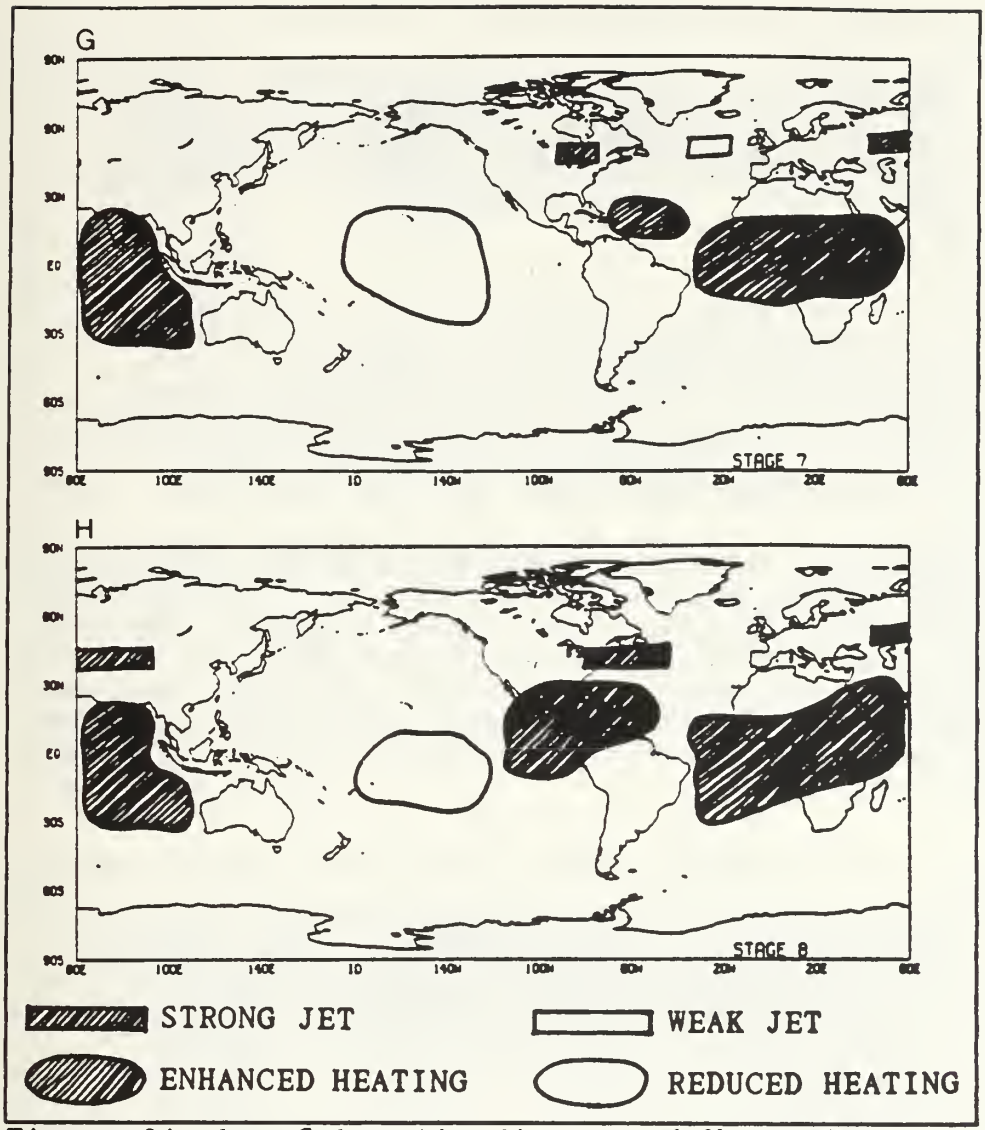

Figure 21g,h. Schematic diagram of North Atlantic jet life-cycle and relationship to global tropical heating. Panels a - h represent Stages 1 through 8, as discussed in Chapter III, Section C.2.

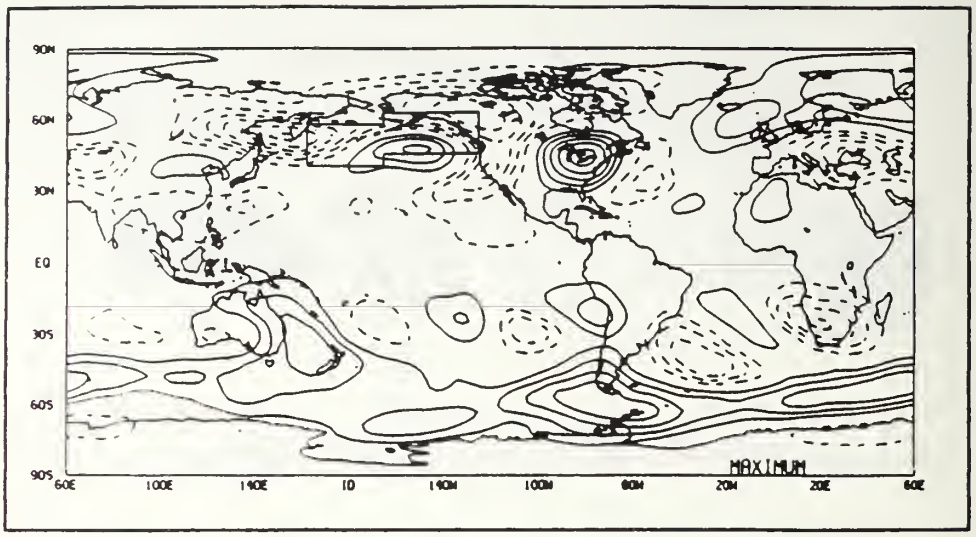

Figure 22. Global 200mb streamfunction anomaly field during the composite PKE anomaly maximum in the North Pacific (NP) boxed region. Contour interval is 2 m^2 s^{-1} with lowest contoured values equal to at ±2 m^2 s^{-1}. Solid (dashed) contours represent positive (negative) streamfunction anomalies which are associated with anticyclonic (cyclonic) flow.

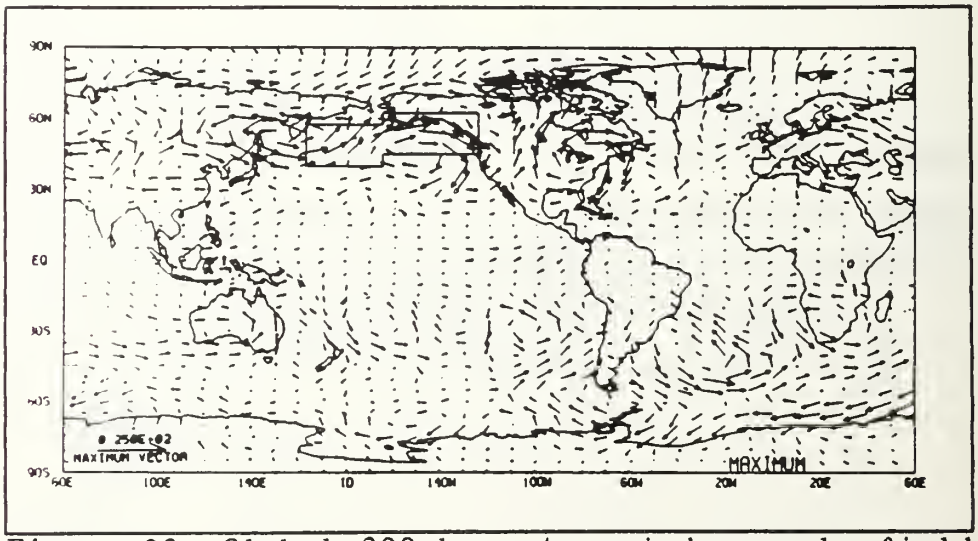

Figure 23. Global 200mb vector wind anomaly field during the composite PKE anomaly maximum in the North Pacific (NP) boxed region.

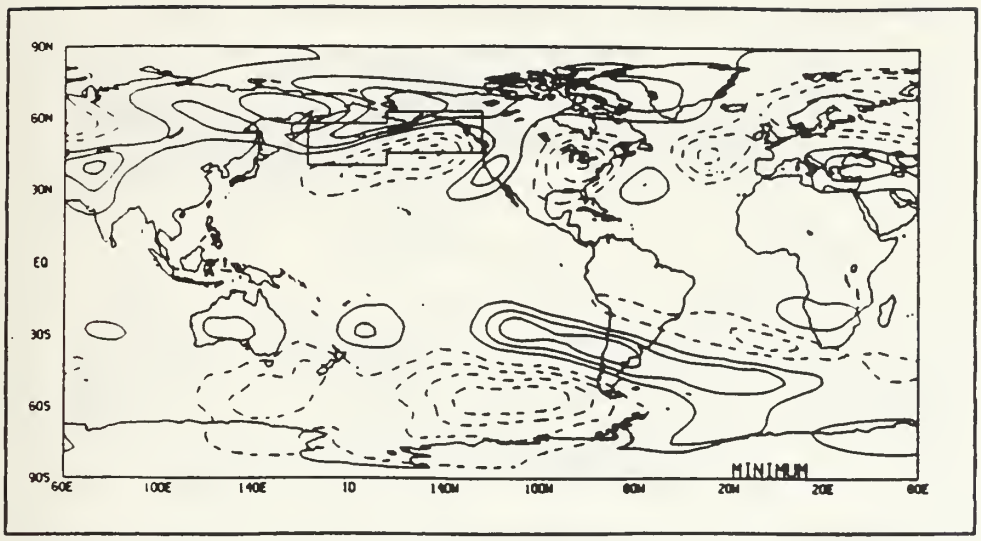

Figure 24. Global 200mb streamfunction anomaly field during the composite PKE anomaly minimum in the North Pacific (NP) boxed region. Contour interval is 2 m^2 s^{-1} with lowest contoured values equal to ±2 m^2 s^{-1}. Solid (dashed) contours represent positive (negative) streamfunction anomalies which are associated with anticyclonic (cyclonic) flow.

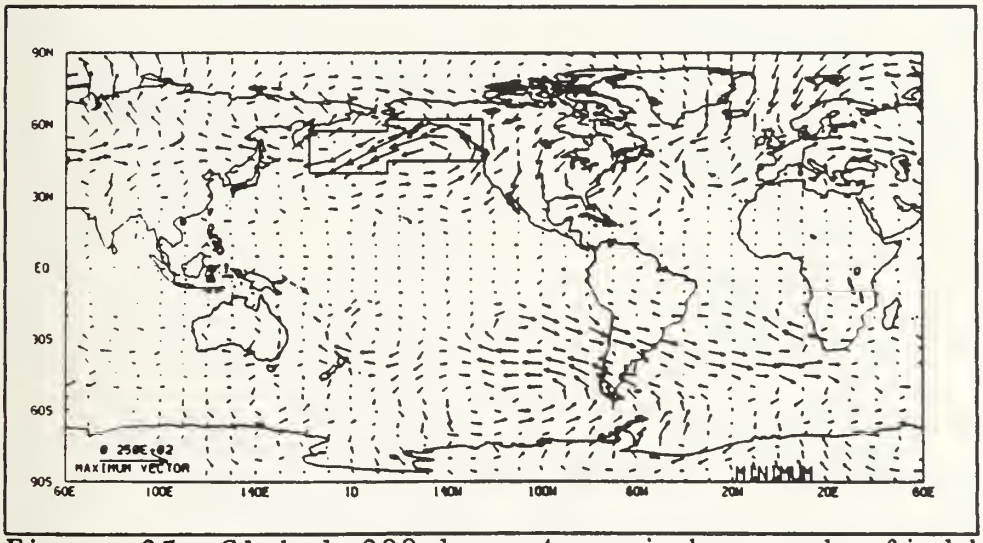

Figure 25. Global 200mb vector wind anomaly field during the composite PKE anomaly minimum in the North Pacific (NP) boxed region.

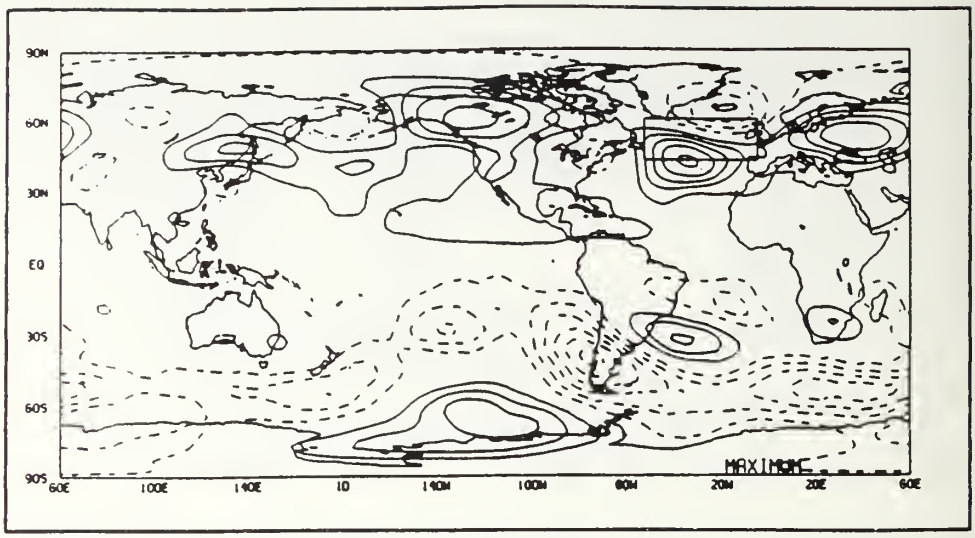

Figure 26. Global 200mb streamfunction anomaly field during the composite PKE anomaly maximum in the North Atlantic (NAT) boxed region. Contour interval is 2 m^2 s^{-1} with lowest contoured value equal to ±2 m^2 s^{-1}. Solid (dashed) contours represent positive (negative) streamfunction anomalies which are associated with anticyclonic (cyclonic) flow.

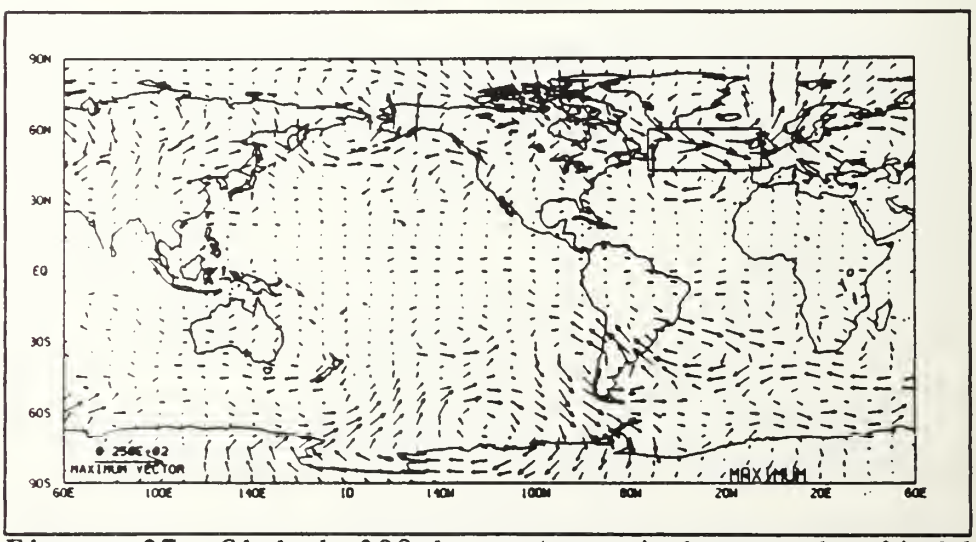

Figure 27. Global 200mb vector wind anomaly field during the composite PKE anomaly maximum in the North Atlantic (NAT) boxed region.

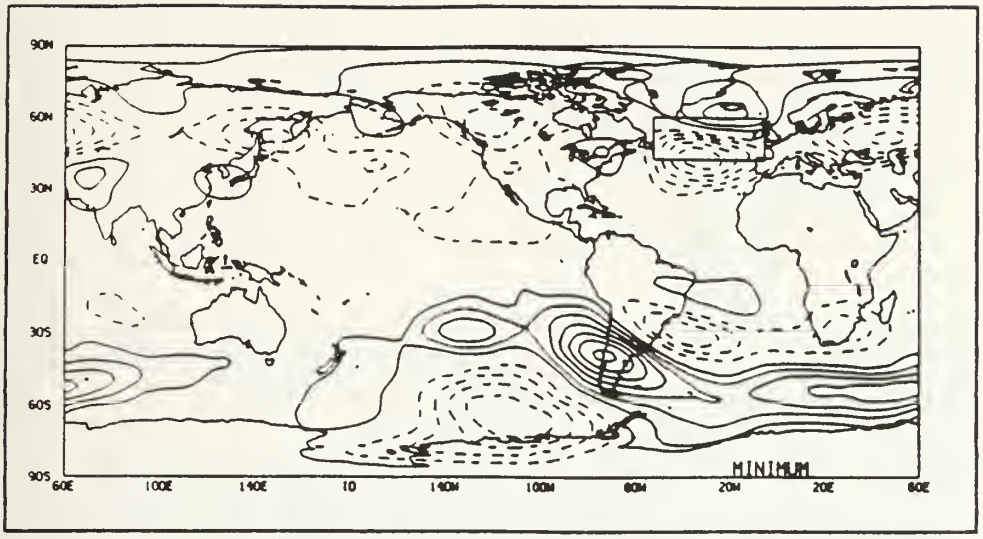

Figure 28. Global 200mb streamfunction anomaly field during the composite PKE anomaly minimum in the North Atlantic (NAT) boxed region. Contour interval is 2 m^2 s^{-1} with lowest contoured value equal to ±2 m^2 s^{-1}. Solid (dashed) contours represent positive (negative) streamfunction anomalies which are associated with anticyclonic (cyclonic) flow.

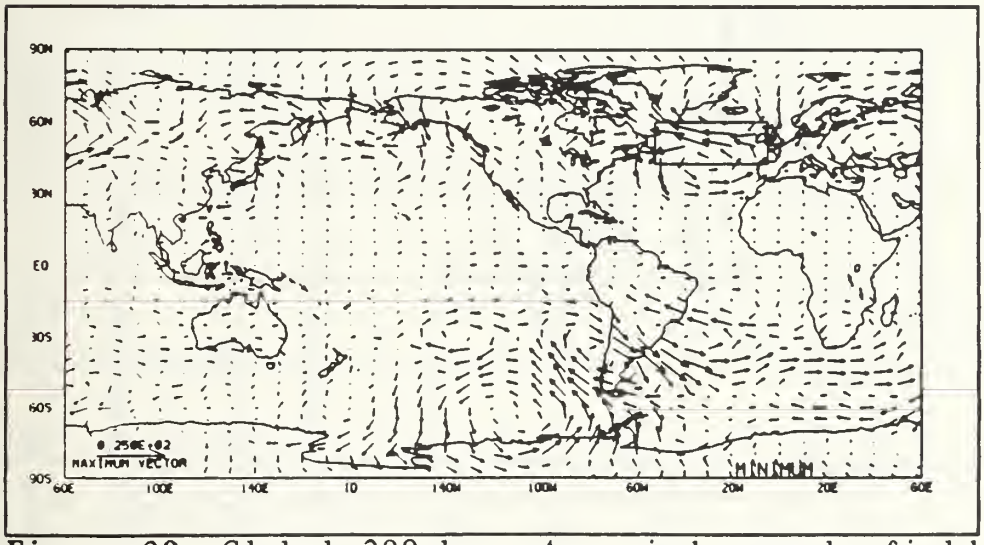

Figure 29. Global 200mb vector wind anomaly field during the composite PKE anomaly minimum in the North Atlantic (NAT) boxed region.

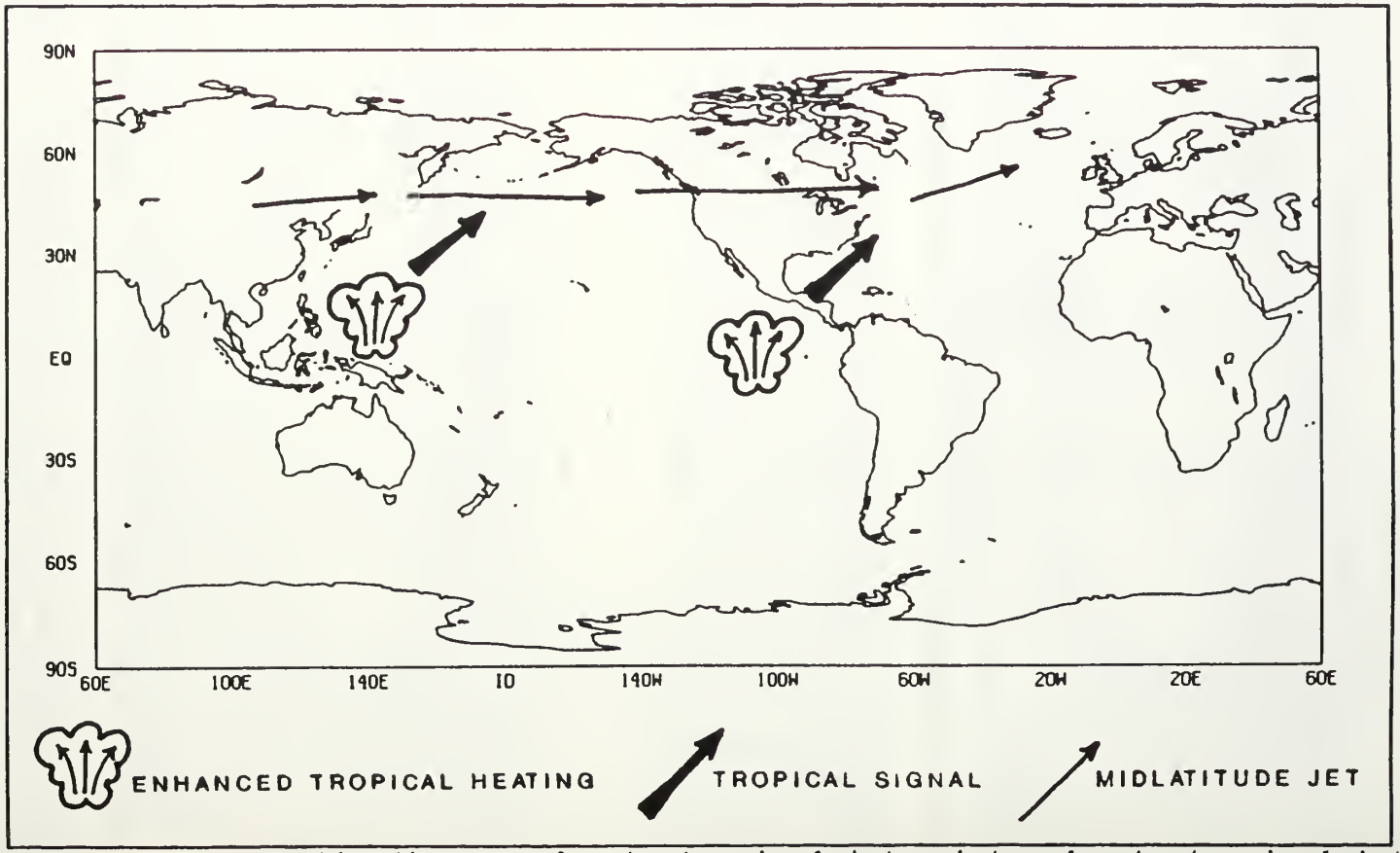

Figure 30. Schematic diagram of extratropical jet - jet and extratropical jet - tropical heating relationships. See discussion in Chapter IV, Section A.

Table 1. NORTH PACIFIC JET LIFE-CYCLE AND RELATIONSHIP TO GLOBAL TROPICAL HEATING ANOMALIES IN SIX REGIONS OF THE TROPICS. THE TROPICAL REGIONS ARE: IO-INDIAN OCEAN, WP-WESTERN PACIFIC, CP-CENTRAL PACIFIC, EP-EASTERN PACIFIC/CARIBBEAN, AT-ATLANTIC, AF-AFRICA. "H" INDICATES ENHANCED HEATING; "C" INDICATES COOLING; "T" INDICATES TRANSITION BETWEEN HEATING AND COOLING.

	IO	WP	CP	EP	AT	AF
STAGE 1 6 days before max	C	H	T	T	T	H
STAGE 2 max	C	H	H	C	H	T
STAGE 3 6 days after max	T	T	H	C	H	T
STAGE 4 12 days after max	H	T	H	T	H	C
STAGE 5 6 days before min	H	C	T	T	T	C
STAGE 6 min	H	C	C	H	T	T
STAGE 7 6 days after min	T	T	C	H	C	H
STAGE 8 12 days after min	C	H	T	T	T	H

Table 2. NORTH ATLANTIC JET LIFE-CYCLE AND RELATIONSHIP TO GLOBAL TROPICAL HEATING ANOMALIES IN SIX REGIONS OF THE TROPICS. THE TROPICAL REGIONS ARE: IO-INDIAN OCEAN, WP-WESTERN PACIFIC, CP-CENTRAL PACIFIC, EP-EASTERN PACIFIC/CARIBBEAN, AT-ATLANTIC, AF-AFRICA. "H" INDICATES ENHANCED HEATING; "C" INDICATES COOLING; "T" INDICATES TRANSITION BETWEEN HEATING AND COOLING.

	IO	WP	CP	EP	AT	AF
STAGE 1 6 days before max	T	T	C	H	T	H
STAGE 2 max	C	H	T	H	C	H
STAGE 3 6 days after max	C	H	H	H	C	T
STAGE 4 12 days after max	C	T	H	T	T	C
STAGE 5 6 days before min	T	C	T	C	T	C
STAGE 6 min	H	C	C	C	T	T
STAGE 7 6 days after min	H	T	C	T	H	H
STAGE 8 12 days after min	H	T	C	H	H	H

APPENDIX B - STATISTICAL SIGNIFICANCE

The procedure used to test the statistical significance of the OLR and KE fields used in this study follows the procedure described by Weickmann et al. (1985).

Percent variance of white noise, in the frequency band of interest, was calculated to be 100% * (3 bins/60 bins) = 5.0%. Red noise background spectra were estimated at each gridpoint from the lag-one autocorrelation. The red noise spectral density at each Fourier frequency is

$$(1 - r^2) / [1 + r^2 - (2 * r * \cos n/N)],$$

where r is the lag-one autocorrelation, n the number of cycles per 120 days, and N is the Nyquist frequency. This spectral density is multiplied by the white noise percent variance to obtain a red noise background. To obtain a 30-60 day background spectrum for percent red noise variance, the spectral density values were averaged over the frequency range of interest (2 - 4 cycles / 120 days). This was then compared to the ratio between the 30-60 day variance and the total variance or percent variance. The percent red noise variance was used as a null hypothesis continuum value for testing the statistical significance of the calculated percent variance using a 99% one-sided chi-squared significance test. Tabulated distribution values, which depend upon the

significance desired and the degrees of freedom, were used in this test.

With three Fourier frequencies in the band of interest and two degrees of freedom per Fourier component, there were six degrees of freedom in the 30-60 day range.

The 99% chi-squared value at 6 degrees of freedom is 16.812. The red noise continuum were multiplied by the ratio 16.812 / 6 = 2.802 to obtain the test statistic with which to compare the percent variance. Multiplying the mean 30-60 day red noise background level by 2.802 yields the percent red noise variance at the 99% significance level.

The percent variance of the OLR and KE fields, in the 30-60 day range, that exceeds the percent red noise variance at the 99% significance level, is shown in Figures 4c and 10c, respectively.

APPENDIX C - COMPOSITE TECHNIQUE

The composite technique is based on the occurrence of relative maxima and minima in the extratropical processed KE (PKE) anomaly time series for a specific region. As shown in Figure 14, for the North Pacific (NP) region, PKE anomaly maxima (minima) occurred on 3 August, and 11 September (28 June, 23 August, and 28 September).

Composite maps were produced by averaging the field of interest (i.e., PKE, POLR, streamfunction, or vector winds) anomaly values at each grid point for all times when there was a relative PKE anomaly maxima (minima) in the NP jet. A similar procedure was used for times before and after extrema.

As an example, to produce the composite POLR anomaly field for the period when PKE was at a maximum in the NP region (Fig. 17c), the POLR anomaly values on 3 August and 11 September were averaged at each grid point. Similarly, on 8 August and 16 September, five days after the maximum, the POLR anomaly values were averaged to produce the composite POLR anomaly field shown in Figure 17d. This composite process was done for each of the 10 days preceding and following the relative PKE anomaly maxima (minima).

LIST OF REFERENCES

Arkin, P.A., and P.E. Ardanuy, 1989: Estimating climate-scale precipitation from space: a review. *J. Climate*, 2, 1229-1238.

Bjerknes, J., 1966: A possible response of the atmospheric Hadley circulation to equatorial anomalies of ocean temperature. *Tellus*, 18, 820-829.

Chang, C.-P., and K.M. Lau, 1982: Short-term planetary-scale interactions over the tropics and midlatitudes during northern winter. Part 1: Contrasts between active and inactive periods. *Mon. Wea. Rev.*, 110, 933-946.

____, and K.G. Lum, 1985: Tropical-midlatitude interactions over Asia and the western Pacific Ocean during the 1983/84 northern winter. *Mon. Wea. Rev.*, 113, 1345-1358.

Ferranti, L., T.N. Palmer, F. Molteni, and E. Klinker, 1990: Tropical-extratropical interaction associated with the 30-60 day oscillation and its impact on medium and extended range prediction. *J. Atmos. Sci.*, 47, 2177-2199.

Gilman, D.L., F.J. Fuglister, and J.M. Mitchell Jr., 1963: On the power spectrum of red noise. *J. Atmos. Sci.*, 20, 182-184.

Ghil, M., and K. Mo, 1991: Intraseasonal oscillations in the global atmosphere. Part I: Northern Hemisphere and tropics. *J. Atmos. Sci.*, 48, 752,-779.

Harr, P., 1993: Observed variability in large-scale circulation anomalies over the tropical western Pacific. To be submitted to *J. Atmos. Sci.*, 1993.

Hurrell J.W. and D.G. Vincent, 1990: Relationship between tropical heating and subtropical westerly maxima in the Southern Hemisphere during SOP-1, FGGE. *J. Climate*, 3, 751-768.

____, and ____, 1991: On the maintenance of short-term subtropical wind maxima in the Southern Hemisphere during SOP-1, FGGE. *J. Climate*, 4, 1009-1021.

Kiladis, G.N., and K.M. Weickmann, 1992: Circulation anomalies associated with tropical convection during northern winter. *Mon. Wea. Rev.*, 120, 1900-1923.

Knutson, T.R., K.M. Weickmann and J.E. Kutzbach, 1986: Global-scale intra-seasonal oscillations of outgoing longwave radiation and 250mb zonal wind during Northern Hemisphere summer. *Mon. Wea. Rev.*, 114, 605-623.

____, and ____, 1987: 30-60 day atmospheric oscillations: Composite life cycles of convection and circulation anomalies. *Mon. Wea. Rev.*, 115, 1407-1436.

Krishnamurti, T.N., and S. Gadgil, 1985: On the structure of the 30 to 50 day mode over the globe during FGGE. *Tellus*, 37A, 336-360.

Lau, K.-M., C.-P. Chang and P.H. Chan, 1983: Short-term planetary-scale interactions over the tropics and midlatitudes. Part II: Winter-MONEX period. *Mon. Wea. Rev.*, 111, 1372-1388.

Lau, N.-C., I.M. Held, and J.D. Neelin, 1988: The Madden-Julian oscillation in an idealized general circulation model. *J. Atmos. Sci.*, 45, 3810-3832.

Madden, R., and P. Julian, 1971: Detection of a 40-50 day oscillation in the zonal wind. *J. Atmos. Sci.*, 28, 702-708.

____, and ____, 1972: Description of global-scale circulation cell in the tropics with a 40-50 day period. *J. Atmos. Sci.*, 29, 1109-1123.

Miller, E.J., *The Impact of a Typhoon on the Global Atmospheric Circulation*, Master's Thesis, Naval Postgraduate School, Monterey, California, December 1992.

Murphree, T., and R. Gelaro, 1992: Mechanisms for intraseasonal variations in tropical - extratropical teleconnections. To be submitted to *J. Atmos. Sci.*, December 1992.

Nitta, T., 1987: Convective activities in the tropical western Pacific and their impact on the northern hemisphere summer circulation. *J. Meteor. Soc., Japan*, 65, 373-390.

Nogues-Paegle, J., and K.C. Mo, 1988: Transient response of the Southern Hemisphere subtropical jet to tropical forcing. *J. Atmos. Sci.*, 45, 1493-1508.

Rosmond, T.E. and T.F. Hogan, 1991: The description of the Navy's Operational Global Atmospheric Prediction Systems (NOGAPS) spectral forecast model. *Mon. Wea. Rev.*, 119, 1786-1845.

Sardeshmukh, P.D., and B.J. Hoskins, 1988: The generation of global rotational flow by steady idealized tropical divergence. *J. Atmos. Sci.*, 45, 1228-1251.

Slingo, J.M., and R.A. Madden, 1991: Characteristics of the tropical intraseasonal oscillation in the NCAR community climate model. *Q. J. R. Meteorol. Soc.*, 117, 1129-1169.

Tribbia, J.J., *Teleconnections Linking Worldwide Climate Anomalies*, pp.285-308, Cambridge University Press, 1991. The rudimentary theory of atmospheric teleconnections associated with ENSO.

Webster, P.S., 1981: Mechanisms determining the atmosphere;s response to sea surface temperature anomalies. *J. Atmos. Sci.*, 38, 554-571.

Weickmann, K.M., G.R. Lussky and J.E. Kutzbach, 1985: Intraseasonal (30-60 day) fluctuations of outgoing longwave radiation and 250mb streamfunction during northern winter. *Mon. Wea. Rev.*, 113, 941-961.

INITIAL DISTRIBUTION LIST

		No. Copies
1.	Defense Technical Information Center Cameron Station Alexandria, VA 22304-6145	2
2.	Library, Code 52 Naval Postgraduate School Monterey, CA 93943-5000	2
3.	Chairman (Code OC/Co) Department of Oceanography Naval Postgraduate School Monterey, CA 93943-5000	1
4.	Chairman (Code MR/Hy) Department of Meteorology Naval Postgraduate School Monterey, CA 93943-5000	1
5.	Professor Thomas Murphree Department of Meteorology Naval Postgraduate School Monterey, CA 93943-5000	1
6.	Professor C.-P. Chang Department of Meteorology Naval Postgraduate School Monterey, CA 93943-5000	1
7.	LT M. T. Neith Naval Oceanography Command Detachment Willow Grove Naval Air Station Willow Grove, PA 19090-5010	1
8.	Commander Naval Oceanography Command Stennis Space Center MS 39529-5000	1
9.	Commanding Officer Naval Oceanography Office Stennis Space Center MS 39529-5001	1

10. Commanding Officer 1
Fleet Numerical Oceanography Center
Monterey, CA 93943-5005

11. Commanding Officer 1
Naval Oceanography and Atmospheric
Research Laboratory
Stennis Space Center
MS 39529-5004

12. Dr. R. Gelaro, Ph.D. 1
Naval Research Laboratory
Monterey, CA 93943-5006

13. Library Acquisitions 1
National Center for Atmospheric Research
P. O. Box 3000
Boulder, CO 80307